frontiers | Frontiers in Earth Science

TYPE Review
PUBLISHED 01 September 2022
DOI 10.3389/feart.2022.932588

OPEN ACCESS

EDITED BY
Hossein Azizi,
University of Kurdistan, Iran

REVIEWED BY
Fan Yang,
Lanzhou University, China
Federico Lucci,
University of Bari Aldo Moro, Italy

*CORRESPONDENCE
Darío Torres-Sánchez,
dtorress@igeofisica.unam.mx

SPECIALTY SECTION
This article was submitted to Petrology, a section of the journal Frontiers in Earth Science

RECEIVED 30 April 2022
ACCEPTED 08 August 2022
PUBLISHED 01 September 2022

CITATION
Torres-Sánchez D, Sosa-Ceballos G, Bolós X and Macías JL (2022), Petrogenesis of mafic-intermediate magmatism of the Michoacán–Guanajuato volcanic field in Western Mexico. A geochemical review. *Front. Earth Sci.* 10:932588. doi: 10.3389/feart.2022.932588

Petrogenesis of mafic-intermediate magmatism of the Michoacán–Guanajuato volcanic field in Western Mexico. A geochemical review

Darío Torres-Sánchez[1]*, Giovanni Sosa-Ceballos[1], Xavier Bolós[2] and José Luis Macías[1]

[1]Instituto de Geofísica, Unidad Michoacán, Universidad Nacional Autónoma de México, Morelia, Michoacán, México, [2]Institute of Geophysics and Planetology, University of Hawai, Honolulu, HI, United States

The Michoacán–Guanajuato volcanic field (MGVF) in the western Trans-Mexican Volcanic Belt is one of the largest and most diverse monogenetic volcanic fields in the world holding more than 1200 volcanic vents. Its eruptive activity goes back to 7 Ma, it is considered an active volcanic field, and the composition of its rocks varies from mafic to silicic. It is essential to understand the geochemical evolution of its products, the complex petrogenetic processes, and the origin of magmas in central Mexico. Although these processes are linked to the subduction of the Cocos plate beneath the North American plate, the magmatic plumbing system of the MGVF remains not completely understood. The MGVF has been studied for decades, focusing in its dominant intermediate magmas. Nevertheless, the origin and evolution of the mafic components and their relation with the intermediate rocks have been poorly discussed. Here, we compile geological and geochemical data of the MGVF to discuss the petrogenesis of mafic magmas along the volcanic field and the role they play in the generation of intermediate melts. We used data published for 429 samples of mafic and intermediate volcanic rocks. Conventional procedures and statistical techniques were used to process the dataset. We propose that MGVF mafic magmas are derived from low degrees (~1–15%) of partial melting of a spinel-bearing lherzolite source/mantle related to the rapid ascent of the asthenosphere caused by an extensional regime that is present in the area. In contrast, intermediate magmas where divided into two main groups based on the Mg content: high-Mg intermediate rocks, which seems to be derived from different rates of assimilation and fractional crystallization process, and low-Mg intermediate rocks, which can be related to fractional crystallization of mafic magmas. In addition, mafic and intermediate magmas display a chemical diversity which is related to mantle heterogeneity domains in the mantle wedge.

KEYWORDS

geochemistry, isotopes, partial melting, mixing process, Michoacán–Guanajuato, Mexico

1 Introduction

The Trans-Mexican Volcanic Belt (TMVB) is a magmatic province in North America, which extends from the Gulf of Mexico to the Pacific coast (Figure 1A; Robin, 1982; Verma, 2000; Gómez-Tuena et al., 2007; Ferrari et al., 2012; Verma, 2015).

Different tectonic models have been proposed and debated to explain the evolution and genesis of the TMVB (Márquez et al., 1999a, 1999b; Ferrari and Rosas-Elguera, 1999; Sheth et al., 2000; Blatter et al., 2001; Ferrari et al., 2002; Verma, 2002; Torres-Alvarado and Verma, 2003; Gómez-Tuena et al., 2018). Some of these models include the conventional subduction-related origin (e.g., Molnar and Sykes, 1969; Negendank et al., 1985; Suarez and Singh, 1986; Pardo and Suárez, 1995; Gómez-Tuena et al., 2003; Carrasco-Núñez et al., 2005), as well as alternative models such as a fracture-related origin (e.g., Mooser and Maldonado-Koerdel, 1961; de Cserna, 1971), rift-related origin (e.g., Shet et al., 200; Márquez et al., 2001; Velasco-Tapia and Verma 2013; Verma, 2002, 2004, 2009, 2015), plume-related origin (e.g., Moore et al., 1994; Márquez et al., 1999a), and slab-detachment model (Ferrari, 2004).

Several monogenetic volcanic fields extend across the TMVB, such as Mascota, Acatlán, Sierra de Chichinautzin, Valle de Bravo, and Xalapa (e.g., Gómez-Tuena et al., 2007; Ferrari et al., 2012). The biggest monogenetic volcanic field in the TMVB is the Michoacán–Guanajuato volcanic field (MGVF; Figure 1B). In addition, the MGVF is one of the most prominent monogenetic volcanic areas in the world in terms of size, variety of volcanic styles, and magma compositions (Hasenaka and Carmichael, 1985).

Previous studies in the MGVF have focused on its geochemical characterization, geochronology, petrology, and eruptive dynamics (e.g., Luhr and Lazzar, 1985a; Luhr and Carmichael, 1985b; Hasenaka and Carmichael, 1987; Luhr et al., 1989; Cébria et al., 2011; Chevrel et al., 2016; Rasoazanamparany et al., 2016; Larrea et al., 2017, 2019; Losantos et al., 2017; Avellán et al., 2020; Bólos et al., 2020; Bólos et al., 2021; Ramírez-Uribe et al., 2021; Reyes-Guzmán et al., 2021; Sosa-Ceballos et al., 2021). Nevertheless, the petrogenesis and relation of the mafic and intermediate volcanic rocks of the MGVF and their tectonic implication with the TMVB is still a debated topic (e.g., Luhr and Lazzar, 1985a; Luhr and Carmichael, 1985b; Hasenaka and Carmichael, 1987; Luhr et al., 1989; Cébria et al., 2011; Chevrel et al., 2016; Hernández-Bernal et al., 2016; Rasoazanamparany et al., 2016; Losantos et al., 2017; Ramírez-Uribe et al., 2021; Sosa-Ceballos et al., 2021). In this work, we compiled published bulk rock compositions, mineral chemistry, and isotopic data from all over the MGVF and evaluated geochemical models to contribute to unravel the petrogenesis of magmas in Mexico.

2 Geological setting

The TMVB is an E-W continental volcanic arc originated by the oblique convergence of the Cocos, Rivera, and North American plates (Demant 1978; Ferrari and Rosas-Elguera, 1999). It is defined as a Miocene–Holocene volcanic province, comprising ~8000 volcanic structures, that extends over ~1000 km long across the central part of Mexico (Ferrari

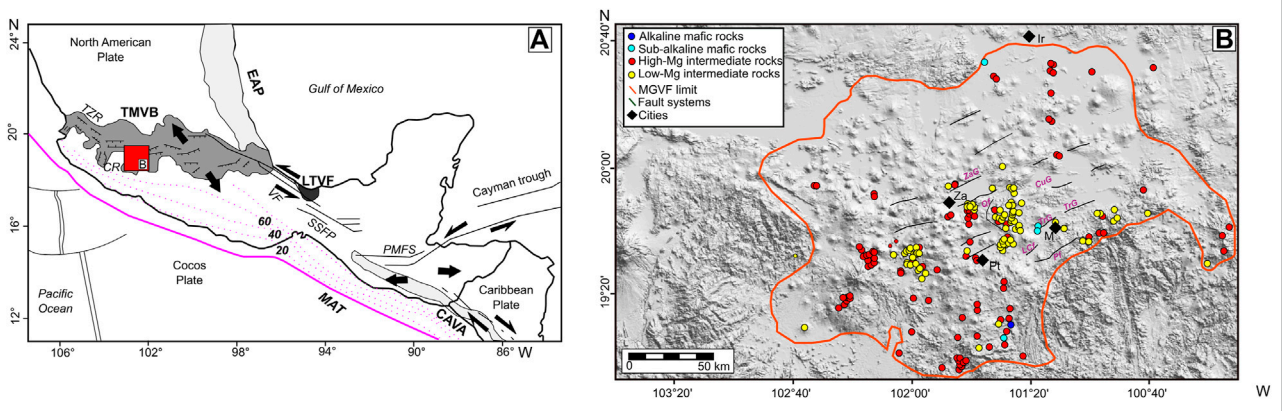

FIGURE 1
(A) Map of the Trans-Mexican Volcanic Belt (TMVB) along with the plate tectonic setting of southern Mexico (modified after Verma, 2015), showing the MGVF area (red square box). The numbers 20, 40, and 60 represent the depth in km of the subducted slab beneath the southern region of Mexico. Faults and fracture zones: TZR, Tepic-Zacoalco Rift; CR, Colima Rift; ChR, Chapala Rift; TCFS, Tula–Chapala fault system; VF, Veracruz fault; SSFP, Strike-Slip fault province; PMFS, Polochic–Motagua fault system; and GCA, graben of Central America. Abbreviations: T, Tepic; V, Veracruz; EAP, Eastern Alkaline Province; LTVF, Los Tuxtlas Volcanic Field; MAT, Middle America Trench; and CAVA, Central American Volcanic Belt. The thick black arrows represent relative motions at plates. The strike-slip vectors and other normal faults are also shown schematically. **(B)** Michoacán–Guanajuato volcanic field (MGVF) showing the mafic and intermediate volcanic rocks. Abbreviations: M, Morelia; Pt, Pátzcuaro; Ir, Irapuato; Za, Zacapu. TrG, Tarímbaro graben; LCf, La Colina fault; Pf, Paloma fault; CuG, Cuitezeo half graben; ZaG, Zacapu graben; and Qf, Quiroga fault.

et al., 2012; Velasco-Tapia and Verma, 2013; Ortega-Gutiérrez et al., 2014; Verma et al., 2013).

The MGVF is one of the largest monogenetic volcanic fields on Earth covering ~40,000 km^2, in the west-central section of the TMVB (Hasenaka and Carmichael, 1985; Valentine and Connor, 2015; Sosa-Ceballos et al., 2021). It contains the youngest continental volcano in Mexico, Paricutin cinder cone (Foshang and González, 1956; Cebriá et al., 2011; Rowe et al., 2011; Larrea et al., 2017; Bolós et al., 2021, 2021). It consists in more than 1200 vents with a large variety of volcanic structures, such as scoria cones, maar craters, medium-size shield volcanoes, lava domes, and lava flows (Hasenaka and Carmichael 1987; Hasenaka 1994; Guilbaud et al., 2012; Mahgoub et al., 2017; Bolós et al., 2021; Sosa-Ceballos et al., 2021).

The MGVF occurs in an extensional tectonic environment which may be related to the sinistral rotation of the Michoacán block due to the oblique convergence of the Cocos plate relative to the North American plate (Singh and Pardo, 1993; Sosa-Ceballos et al., 2021). The MGVF is constrained by two main fault systems: the Morelia–Acambay with ENE-WSW and NE trending faults and the Taxco–San Miguel with NNW-SSE and NW-SE striking faults (Alanís-Álvarez et al., 2002; Sosa-Ceballos, et al., 2021). The structural system between these two main faults consists of a complex arrangement of fault zones that control the kinematics of different regional blocks (e.g., Johnson and Harrison, 1989, 1990; Pasquaré et al., 1991; Garduño-Monroy et al., 2009; Guilbaud et al., 2012; Kshirsagar et al., 2016; Sosa-Ceballos et al., 2021). The magmatic distribution of the MGVF might be controlled by this tectonic configuration (e.g., Bolós et al., 2020; Gómez-Vasconcelos et al., 2020).

The magmatism of the MGVF started in the Late Pliocene, although its activity increases from the Pleistocene through the Holocene (Hasenaka and Carmichael 1985; Ban et al., 1992; Guilbaud et al., 2012; Siebe et al., 2014; Pola et al., 2015; Osorio-Ocampo et al., 2018). Hasenaka and Carmichael (1985) estimated a magma discharge rate of 0.8 km^3/1 ka for the last 40 ka in the whole MGVF. However, Guilbaud et al. (2012) proposed rates from 0.34 to 0.39 km^3/1 ka for the last 10 ka in the Tacámbaro zone (10% of the entire MGVF), suggesting a highly variable magma discharge rate in space and time, or heterogeneous spatial distribution of volcanoes (Guilbaud et al., 2011).

The youngest volcanic activity within the MGVF occurred at Jorullo (1759–1774) and Parícutin (1943–1952) volcanoes, both located in zones with a high density of volcanic vents (Hasenaka and Carmichael 1985; Guilbaud et al., 2011). The occurrence of these young volcanoes and the two recent seismic swarms in 2020 and 2021 in the Uruapan area highlights the high probability of a new monogenetic eruption in the short to medium term within this region.

Most of the magmas that erupted in the MGVF belong to the calc-alkaline series, characteristic of subduction zones (Hasenaka and Carmichael 1987; Gómez-Tuena et al., 2005; Bolós et al., 2015; Gómez-Tuena et al., 2018). However, there are some volcanic products that belong to the alkaline series, distinctive from primitive OIB magmas (Hasenaka and Carmichael 1987), especially in the northern part of the MGVF (Ortega-Gutierrez et al., 2014; Losantos et al., 2015). The rocks of the MGVF are predominantly intermediate, and 40% of all known rocks are andesites and 33% are basaltic andesites (Sosa-Ceballos et al., 2021). Previous studies proposed that the mafic and intermediate magmas erupted were derived from partial melting of a heterogeneous mantle contaminated with subducted sediments and oceanic crust (Gilbaud et al., 2019; Larrea et al., 2021), partial melting of the deep crust (Ownby et al., 2011), assimilation and fractional crystallization (AFC) processes (McBirney and TaylorArmstrong, 1987; Agrawal et al., 2008; Ceibrá et al., 2011; Losantos et al., 2017), and fractional crystallization (Luhr and Carmichael, 1985b; Johnson et al., 2008). According to Sosa-Ceballos et al. (2021), felsic magmas could be related to the accumulation of intermediate magmas and the assimilation of granodiorites–granites favored by extensional–transtensional tectonics within the upper crust (e.g., Pérez-Orozco et al., 2018).

3 Database and processing procedures

The database from mafic and intermediate volcanic rocks from the MGVF was constructed from different literature sources. Major element composition, including rare earth element and trace element compositions, of 429 samples (Supplementary Tables S2, S3) were compiled from Anderson et al. (1974; n = 1); Avellan et al. (2020; n = 13); Carmichael et al. (2006; n = 4); Cebria et al. (2011; n =12); Chesley et al. (2002; n =12); Chevrel et al. (2016; n = 27); Corona-Chavez et al. (2006; n = 2); Freydier et al. (2000; n = 8); Gomez-Vasconcelos et al. (2015; n = 17); Guilbaud et al. (2019; n = 12); Hasenaka and Carmichael (1985; n = 5); Hasenaka and Carmichael (1987; n = 26); Hernández-Bernal et al. (2016; n = 5); Kshirsagar et al. (2015; n = 30); Lapierre et al. (1992; n = 3); Larrea et al. (2017; n =7); Larrea et al. (2019; n = 18); Lassiter and Luhr (2001; n = 2); Losantos et al. (2014; n = 11); Losantos et al. (2017; n = 47); Luhr and Lazzar, 1985a; n = 10); Luhr and Carmichael, 1985b; n = 10); Luhr et al. (1989; n = 4); McBirney and TaylorArmstrong, 1987; n = 11); Perez-Orozco et al. (2018; n = 10); Ramírez-Uribe et al. (2019; n = 26); Ramírez-Uribe et al. (2021; n = 13); Rasoazanamparany et al. (2016; n = 27); Rowe et al. (2011; n = 10); Verma and Hasenaka (2004; n = 28); and Wilcox (1954; n = 18).

Isotopic data (Sr-Nd and Pb) of 142 samples were compiled from Anderson et al. (1974; n = 1); Cebria et al. (2011; n = 12); Chesley et al. (2002; n = 12); Chevrel et al. (2016; n = 6); Guilbaud et al. (2019; n = 12); Hernández-Bernal et al. (2016; n = 3); Lapierre et al. (1992; n = 2); Lassiter and Luhr (2001; n = 4); Losantos et al. (2017; n = 33); Luhr et al. (1989; n = 2); McBirney and TaylorArmstrong, 1987; n = 11); Rasoazanamparany et al. (2016; n = 26); Verma and Verma (2018; n = 17).

Major element compositions were processed using the IgRoCS software (Verma and Rivera-Gómez, 2013), to assign rock nomenclature according to the IUGS (Le Bas et al., 1986; Le Maitre et al., 2002). The use of the IgRoCS software allows the subdivision of Fe into two oxidation varieties (FeO and Fe_2O_3) and the calculation of Fe_2O_3/FeO ratios following the Middlemost (1989) option for Fe oxidation adjustment. The adjustment of the sum to 100% anhydrous basis and the calculation of the CIPW norm as a standard igneous norm, were also achieved with this software. The use of 100% adjusted data on an anhydrous basis and the Fe oxidation adjustment minimizes the effects of analytical errors and element mobility (e.g., post-emplacement alteration and compositional changes during grinding of rock samples in the laboratory; Irvine and Baragar (1971)) and make more reliable and consistent use of the diagram of total alkali versus silica.

In order to report the mean and standard deviation, we used the UDASyss 3.2.2 software (Rosales-Rivera et al., 2019), which is a computer program used for data processing of experimental data. This software has been used in diverse scientific fields (e.g., igneous petrology, geochemistry of sands and sediments, and clinical and cognitive neuroscience). UDASyss 3.2.2 (Rosales-Rivera et al., 2019) comprises a model to calculate statistical parameters and dispersion estimates; in addition, this software is capable of efficiently and automatically applying the recursive discordancy and significance tests (F, t, and ANOVA) for statistical processing of experimental data. Therefore, in the present study, we used this software to develop discordancy tests at a strict 99% confidence level of the mean, which is helpful to determine the most confinable mean and standard deviation values from each rock type from the analyzed dataset (Verma, 2020). Statistical synthesis of geochemical compositional information of mafic and intermediate volcanic rocks is reported in Supplementary Tables S6, S7.

4 Results

4.1 Petrography and mineral chemistry

Previous petrographic studies show that the MGVF mafic rocks display porphyritic textures with mineral assemblages conformed by olivine, plagioclase, clinopyroxene, and orthopyroxene phenocrysts (Hasenaka and Carmichael, 1987; Luhr et al., 1989; Verma and Verma., 2013; Guilbaud et al., 2019). Olivine phenocrysts in mafic volcanic rocks display variable compositions, $Fo_{43–88}$ (Supplementary Table S1; Pola et al., 2014; Larrea et al., 2017; Guilbaud et al., 2019).

Different authors show that intermediate volcanic rocks from the MGVF (Wilcox, 1954; Luhr and Carmichael, 1985b; Hasenaka and Carmichael, 1987; Kelemen, 1995; Verma and Hasenaka, 2004; Chevrel et al., 2016; Reyes-Guzmán et al., 2021) comprise a mineral assemblage characterized by clinopyroxene, dominantly augite and diopside ($Wo_{1–48}$; Supplementary Table S2; Figure 2A), orthopyroxene with clinoenstatite composition ($En_{31–99}$; Supplementary Table S2; Figure 2A), plagioclase with disequilibrium textures and albite–bytownite composition ($An_{3–83}$; Supplementary Table S3; Figure 2B), and scarce olivine phenocryst ($Fo_{62–88}$; Figure 2B; Supplementary Table S1; Wilcox, 1954, Luhr and Carmichael, 1985b; Hasenaka and Carmichael, 1987; Verma and Agrawal, 2011; Chevrel et al., 2016).

4.2 Rock-type classification and major elements

About 5 % of the analyzed rocks ($n = 22$) from the MGVF are mafic, alkaline, and sub-alkaline, with values that display SiO_2 = 47.1–51.6 wt% and Mg# = 34–78 (Supplementary Table S4). Furthermore, 95 % of the analyzed rocks have an intermediate composition with SiO_2 = 50.7–62.9 wt% and Mg# = 32–94. We further divided the intermediate magmatic group into two groups: 1) high-Mg intermediate magmas and 2) low-Mg intermediate magmas.

4.2.1 Mafic magmatic group

Rocks forming this group are basalt and trachybasalt (Figure 3A), some of which have high-K calc-alkaline and shoshonite affinity (Figure 3B). Alkaline mafic rocks displays contents of SiO_2 = 48.3–50.1 wt%; MgO = 4.3–7.5 wt,%; K_2O = 0.9–2.1 wt%; and Mg# = 47–66, whereas sub-alkaline rocks contain SiO_2 = 49.8–51.8 wt%; MgO = 5.5–9.1 wt%; K_2O = 0.1–1.3 wt%; and Mg# = 50–73. Both styles of mafic magmas (alkaline and sub-alkaline) are olivine and diopside normative (Supplementary Tables S4, S7).

4.2.2 High-Mg intermediate magmatic group

This group comprises basaltic andesite, andesite, basaltic trachyandesite, and trachyandesite (Figure 3A) and is mainly composed of confidence levels at 99% (*CL99*) of SiO_2 = 56.1–57.1 wt%; MgO = 5.0–5.4 wt%; K_2O = 1.1–1.2 wt%; and Mg# = 75.1–78.7. This rock group is diopside normative (Supplementary Table S4).

4.2.3 Low-Mg intermediate magmatic group

This group comprises basaltic andesite, andesite, and trachyandesite compositions (Figure 3A). It is characterized by *CL99* values of SiO_2 = 57.1–58.3; MgO= 3.5–3.8; K_2O = 1.6–1.7; and Mg# = 57.4–58.1. Like the other groups, this is diopside normative (Supplementary Table S4).

4.3 Trace and rare earth elements

Average vales of chondrite-normalized rare earth elements (REEs) and trace elements were used to elaborate chondrite-

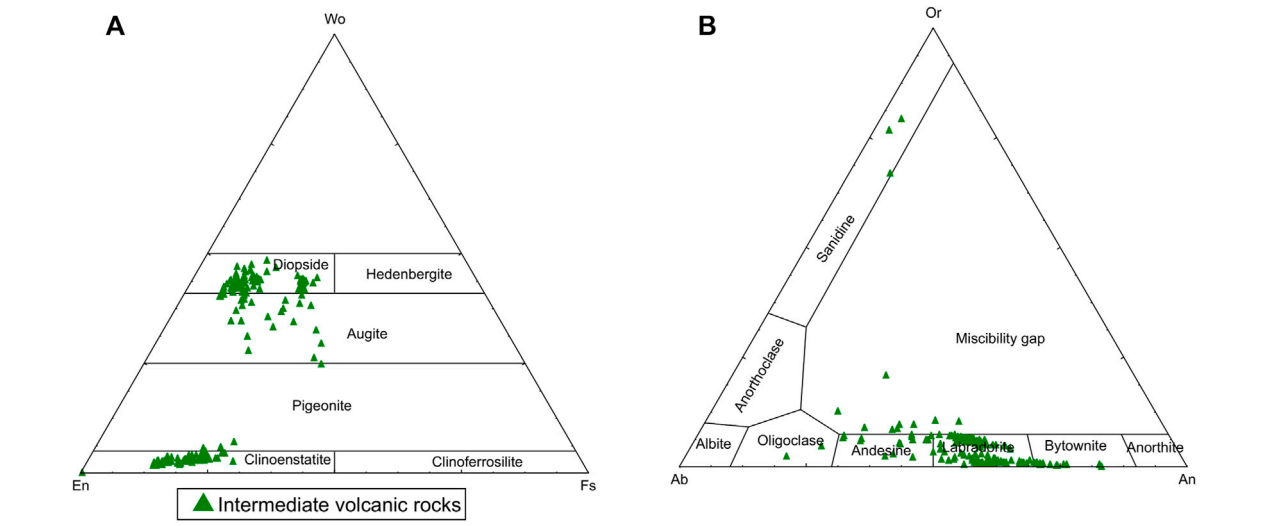

FIGURE 2
(A) Compositional variations of pyroxene from the MGVF intermediate volcanic rocks. Abbreviations: En, enstatite; Fs, ferrosilite; and Wo, wollastonite. **(B)** Compositional variations of feldspar in MGVF intermediate magmas. Abbreviations: An, anorthite; Ab, albite; and Or, orthoclase.

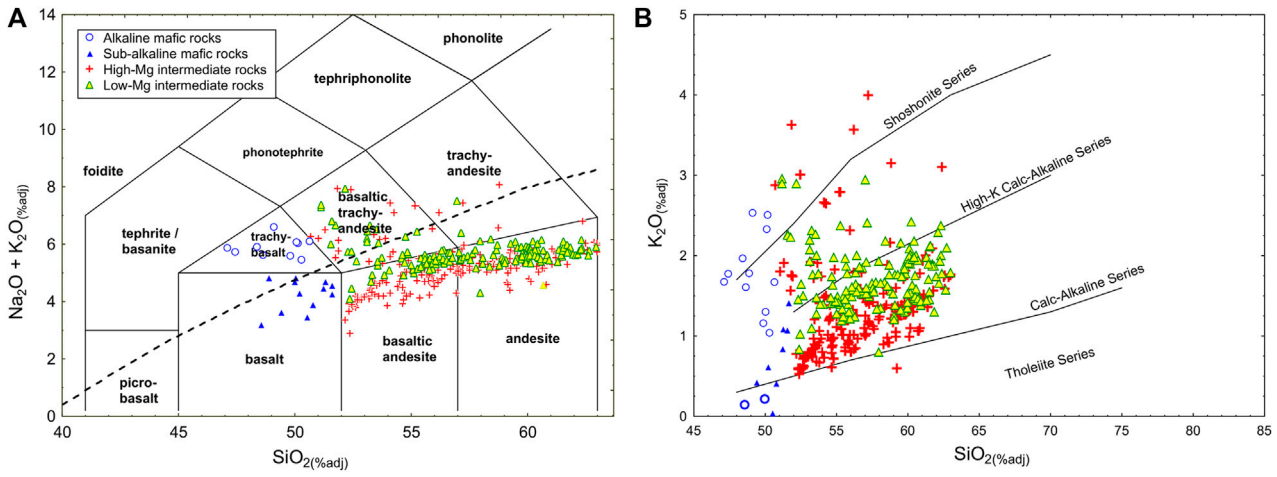

FIGURE 3
(A) Total alkali–silica classification diagram for the volcanic rocks from the MGVF (TAS; Le Bas et al., 1986). **(B)** Bivariate diagram of $K_2O_{(adj)}$–$SiO_{2(adj)}$ diagram of Peccerrillo and Taylor (1976).

normalized REEs diagrams (Figures 4A,C) and multielement-normalized diagrams (Figures 4B,D).

4.3.1 Mafic magmatic group

The mafic magma group exhibit light REE–enriched patterns with a relatively flat heavy REE trend and lacks Eu anomalies ([Eu/Eu]* = 0.8–1.1), where $[Eu/Eu]^* = \sqrt{\frac{(Eu)_{CN}}{(Sm_{CN} \times Gd_{CN})}}$; Supplementary Table S6; Figure 4A). Alkaline mafic rocks display $[La/Yb]_{CN}$ ratios of 2.9–8.6. This group contains a total REE concentration of 79–206 ppm (Supplementary Table S6). Sub-alkaline mafic rocks show $[La/Yb]_{CN}$ ratios of 0.6–5.5 and total REE concentrations of 42–120.3 ppm (Supplementary Table S6).

Primitive mantle–normalized multielement patterns (Figure 4B) show a flat slope between highly incompatible elements and more compatible elements. Alkaline mafic rocks exhibit low Nb [(Nb/Nb* = 0.6–1.2), where Nb/Nb*= $\sqrt{\frac{(Nb)_{CN}}{(Ba_{CN}+La_{CN})}}$, (Verma, 2006)], Ba, and P anomalies.

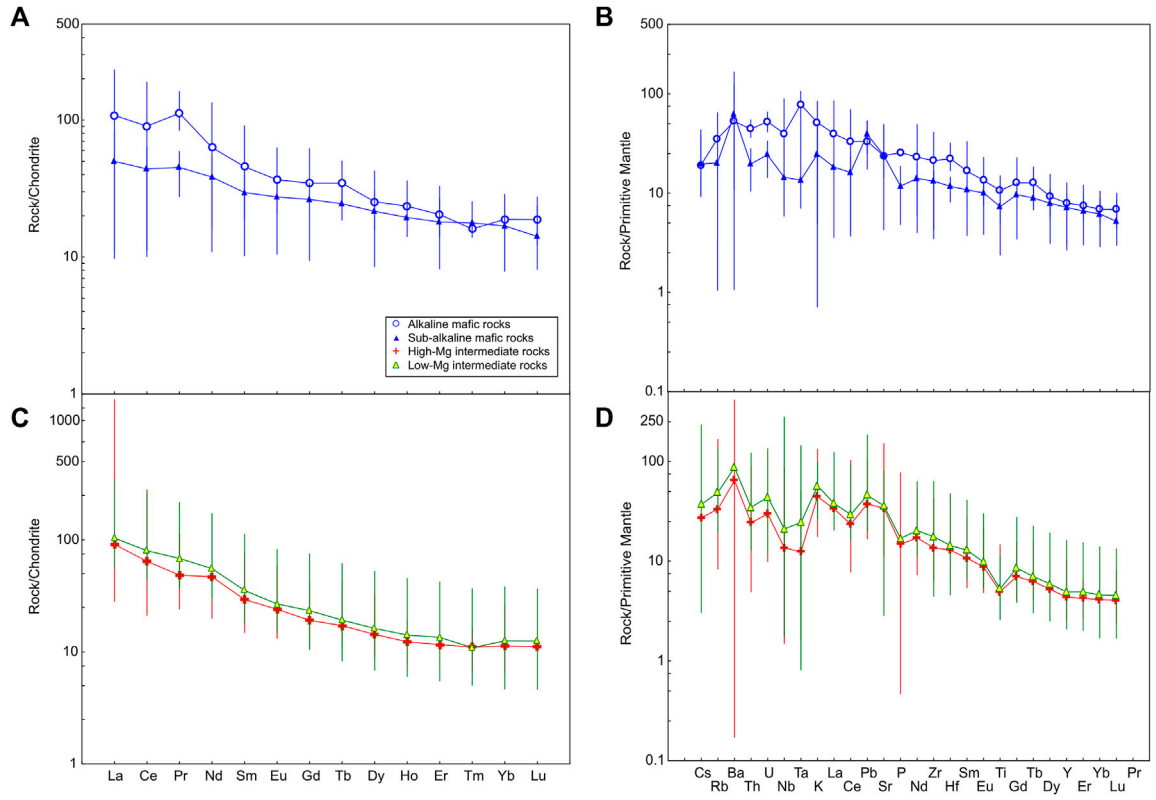

FIGURE 4
(A,B) Chondrite-normalized rare earth element (REE) and primitive mantle–normalized multielement diagram for mafic magmas from MGVF. **(C,D)** Chondrite-normalized rare earth element (REE) and primitive mantle–normalized multielement diagram for intermediate magmas from MGVF. The chondrite and primitive mantle values from normalization are taken from McDonough and Sun (1995).

Verma et al. (2015) and Verma (2020) proposed that Nb anomalies suggest different tectonic setting for volcanic rocks (basic, intermediate, and felsic composition). According to this author, basic rocks from extensional tectonic settings display minor anomalies relative to intermediate and felsic rocks, which are modified by crustal contamination. Otherwise, sub-alkaline mafic rocks display low Nb (Nb/Nb* = 0.2–0.7), Ba, and P anomalies.

4.3.2 High-Mg intermediate magmatic group

Average values of this group present an enrichment in light REE, show a relatively small negative Eu anomaly ([Eu/Eu]* = 0.9–1; $[La/Yb]_{CN}$ = 5.3–6.1), and display a flat pattern in heavy REE (Figure 4C). This group is characterized by total REE concentrations of 72–83.6 ppm. It is remarkable the great similarity between the chondrite-normalized REE patterns of this group and the mafic magmatic group (Figure 4A), especially with the alkaline mafic rocks (Figure 4A).

Primitive mantle–normalized multielement patterns show enrichment in highly incompatible elements with a semi-horizontal trend to more compatible trace elements (Figure 4D). It displays similarities to the mafic magmatic group, especially in the absence of high negative anomalies of high-field strength elements (HFSE; i.e., Nb/Nb* = 0.1–0.2; Supplementary Table S7).

4.3.3 Low-Mg intermediate magmatic group

This magmatic group has an enrichment trend in light REE (Figure 4C), with a LREE–HREE semi-horizontal trend, and lacks negative Eu anomalies ([Eu/Eu]* = 0.8–0.9; $[La/Yb]_{CN}$ = 7.7–8.3; Figure 4C). Total REE concentrations of this group range from 106.3 to 117 ppm (Supplementary Table S7). The primitive mantle-normalized multielement diagram of this group reveals enrichment in highly incompatible elements relative to more compatible elements (Figure 4D). This trend can be comparable to the spectrum of the mafic magmatic group (Figure 4D). Moreover, trace element average concentrations of the low-Mg intermediate magmatic group lack negative anomalies of HFSE (Nb/Nb* = 0.1–0.2; Supplementary Table S7).

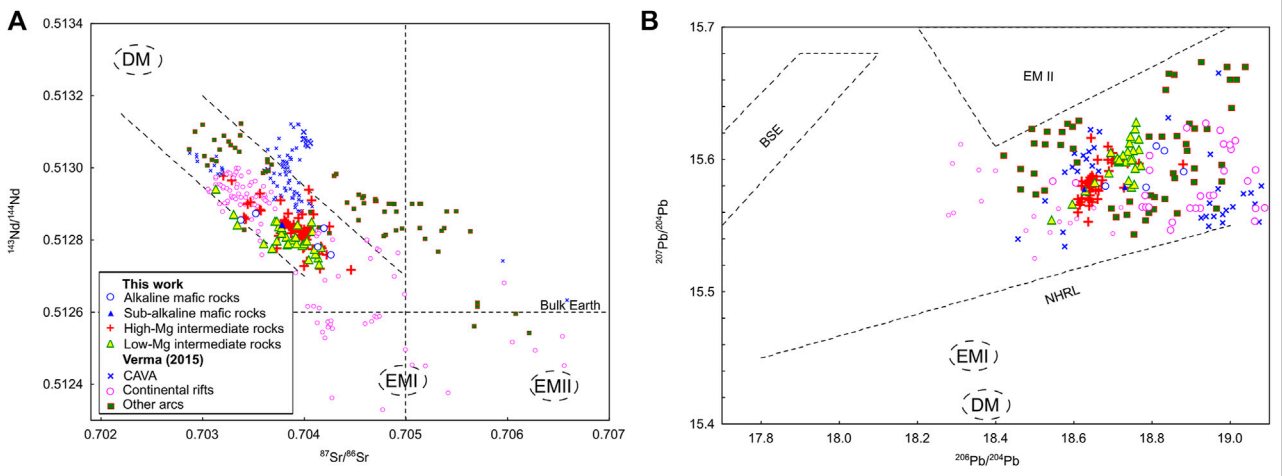

FIGURE 5
(A) Sr–Nd isotope plot for volcanic rocks from MGVF. **(B)** Pb–Pb isotope diagram for volcanic rocks from MGVF. Abbreviations: BSE, bulk silicate Earth; EMII, enriched mantle type-II; and NHRL, Northern Hemisphere Reference Line. BSE and EMII are taken from Faure (1986), and NHRL values are from Zindle and Hart (1986). Data from Central American Volcanic Arc (CAVA), continental rifts (Abu, Gabra, China, East Africa, Ethiopia, Turkey (Kula), Basin and Range, Colorado Plateau, Rio Grande, and Utah), and other arcs (Aleutians, Fiji, Lesser Antilles, Mariana, Papua New Guinea, Philippines, and Sunda-Banda) are form the compilation made by Verma (2015).

4.4 Radiogenic isotopes of Sr, Nd, and Pb

Sr–Nd isotope data of the MGVF mafic and intermediate volcanic rocks (Supplementary Table S5) were plotted in the conventional ($^{87}Sr/^{86}Sr$) vs. ($^{144}Nd/^{143}Nd$) diagram (Figure 5A), together with isotopic data from different island arcs and continental rifts compiled by Verma (2015). The mafic and intermediate magma groups of the MGVF are related to the mantle array (Figure 5A).

Lead isotopic data were plotted in the conventional bivariate diagram of ($^{206}Pb/^{204}Pb$) vs. ($^{207}Pb/^{204}Pb$) (Figure 5B). The MGVF rocks are plotted, same as the Sr–Nd diagram, together with values of different continental rifts and island arcs (Verma, 2015). The Northern Hemisphere Reference Line (NHRL; Zindler and Hart, 1986) was also plotted in this diagram as a reference. On the ($^{206}Pb/^{204}Pb$) vs. ($^{207}Pb/^{204}Pb$) diagram the MGVF mafic and intermediate rocks do not display a systematic difference between them and are mainly plotted between the NHRL line and the EM II field (Figure 5B).

5 Discussion

5.1 Origin of the mafic magmatism

The origin and evolution of the MGVF mafic rocks have been studied in different regions such as in the Jorullo–Tacámbaro zone and in the northwest of the city of Morelia (e.g., Losantos et al., 2017; Guilbaud et al., 2019; Avellán et al., 2020); however, despite the amount of geochemical data available in the literature, such as the study elaborated by Hasaneka and Carmichael (1987), a comprehensive understanding of the volcanic field is still far from being complete. For example, Blatter and Hammersley (2010) developed a complete study of the Tzitzio Gap; however, we lack a study that integrates general observations and structural features with geochemical characteristics and develops quantitative models of mafic volcanic rocks for the volcanic field as a whole. Different authors proposed that mafic rocks could be derived by partial melting of the mantle wedge (e.g., Luhr et al., 1989; Hawkeswoirth et al., 1991; Blatter and Hammersley 2010; Gómez-Tuena et al., 2018). Moreover, Losantos et al. (2017) proposed that low degrees of melting can produce small volumes of alkaline melts from alkaline-enriched portions of the mantle wedge. Luhr et al. (1989) proposed that alkaline magmas were formed during melting events that incorporated components from hydrous metasomatic veins rich in phlogopite, which are formed above the subduction slab. Thus, Lassiter and Luhr (2001), with Os isotopic information, proposed that variable inputs of slab-derived fluids or melts of less evolved magmas display higher $^{187}Os/^{188}Os$ ratios. These authors also suggested that a heterogeneous mantle might have been involved in the generation of magmas in this zone of Mexico.

Although we used bivariate diagrams of immobile trace elements ratios to investigate the source of this mafic magmatic group, the short number of analyzed rocks makes it difficult to suggest the origin of all mafic rocks along the MGVF and determine what type of processes affect their final composition. Despite the lack of a robust dataset, we suggest that the few sub-alkaline mafic rocks might have an N-MORB

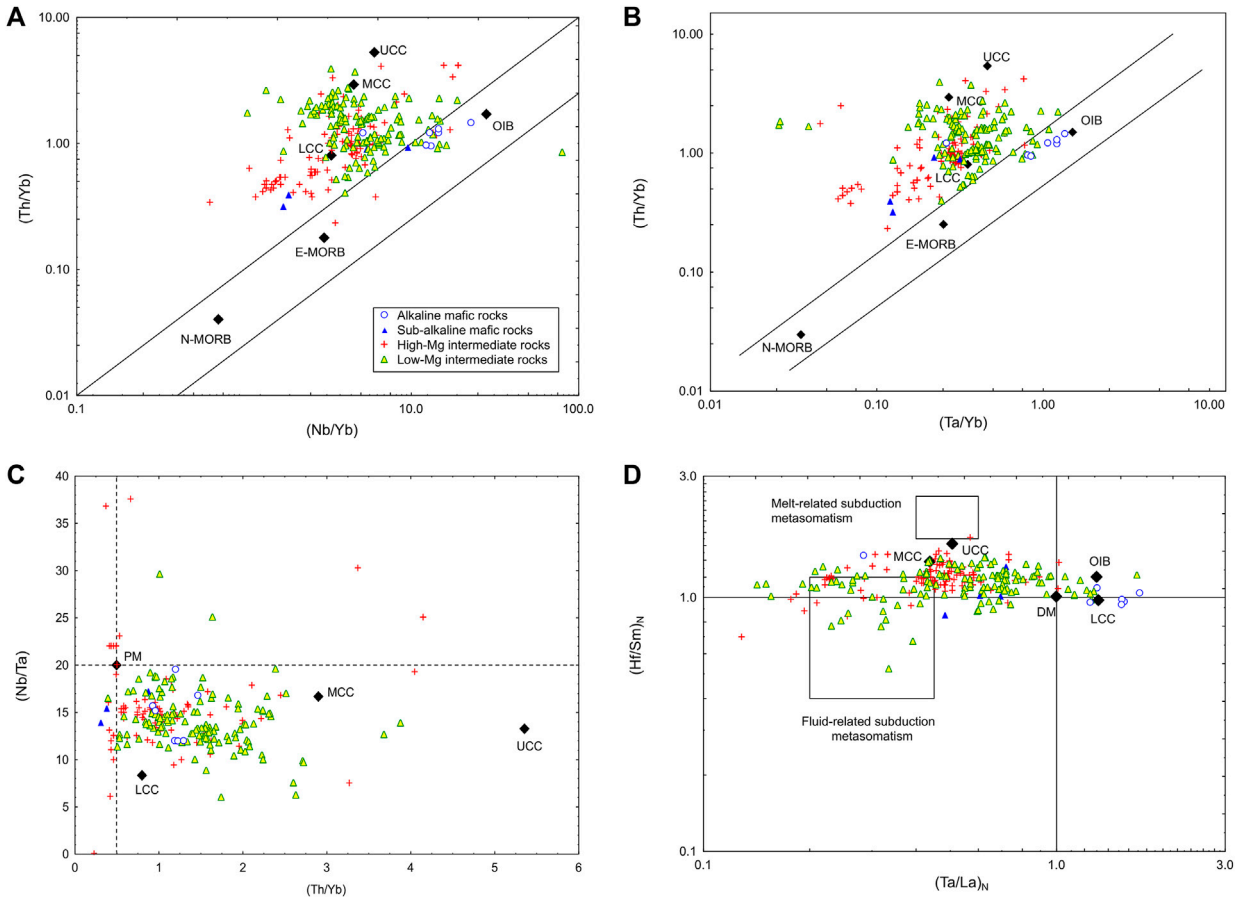

FIGURE 6
(A) (Th/Yb) vs. (Nb/Yb) diagram for the volcanic rocks from the MGVF. **(B)** (Ta/Yb) vs. (Nb/Yb) diagram for the volcanic rocks from the MGVF. **(C)** (Nb/Ta) vs. (Th/Yb) diagram for volcanic rocks from the MGVF. **(D)** $(Hf/Sm)_N$ vs. $(Ta/La)_N$ diagram, melt, and fluid-related subduction metasomatism areas are from La Fléche et al. (1998). Abbreviations: OIB, ocean island basalt; E-MORB, enriched mid-ocean ridge basalt; N-MORB, normal mid-ocean ridge basalt; LCC, lower continental crust; MCC, middle continental crust; UCC, upper continental crust; PM, primitive mantle; and DM, depleted mantle. Continental crust values are taken from Rudnick and Gao (2003). Mantle values are taken from McDonough and Sun (1995).

mantle source that produced magmas that were modified by variable amounts of assimilation of continental crust, which added Nb, Ta, and Th (Figure 6). The same is suggested by REE, where the continental crust additions may have depleted the HREE with respect to more alkaline mafic rocks (Figure 4). Although the alkaline mafic rocks are more closely related with OIB-type values within the mantle array (Figure 6), they are probably mixed with typical sub-alkaline melts (depleting their Nb–Ta and Th values). Isotopic interpretations shows the same problem about sample representativeness; however, it is clear that the alkaline rocks are more radiogenic in Sr and Pb isotopes, which is in accordance to data from alkaline environments (Figure 5).

We also investigated the effects of variable degrees of partial melting and/or fractional crystallization with bivariate diagrams of immobile trace elements ratios (Figure 7). These diagrams point to variable degrees of partial melting rather than fractional crystallization effects (Figure 7). In addition, we noted that the alkaline rocks show a wider range of REE ratios; we suggest that rather than higher degrees of partial melting, this variability reflects variable, and perhaps frequent, mixing events with typical sub-alkaline magmas.

For a better understanding of the processes that control the genesis of the mafic group, a quantitative analysis was performed following the modeling approach of Zou (2007). This model uses batch partial melting equations to represent the origin of partial melting that dominates in the mafic magmatic group. Due to the scarcity of mantle xenoliths from the study area, we used REE concentration of garnet- and spinel-bearing lherzolite values proposed by Frey (1980) and McDonough (1990), respectively, as initial magma (C_0). Mineralogical compositions used for spinel-bearing lherzolite melting are based on those proposed by Pearson et al. (2014) and Aguirre-Espinosa et al. (2022): 0.66 Ol + 0.24 Opx + 0.08 Cpx

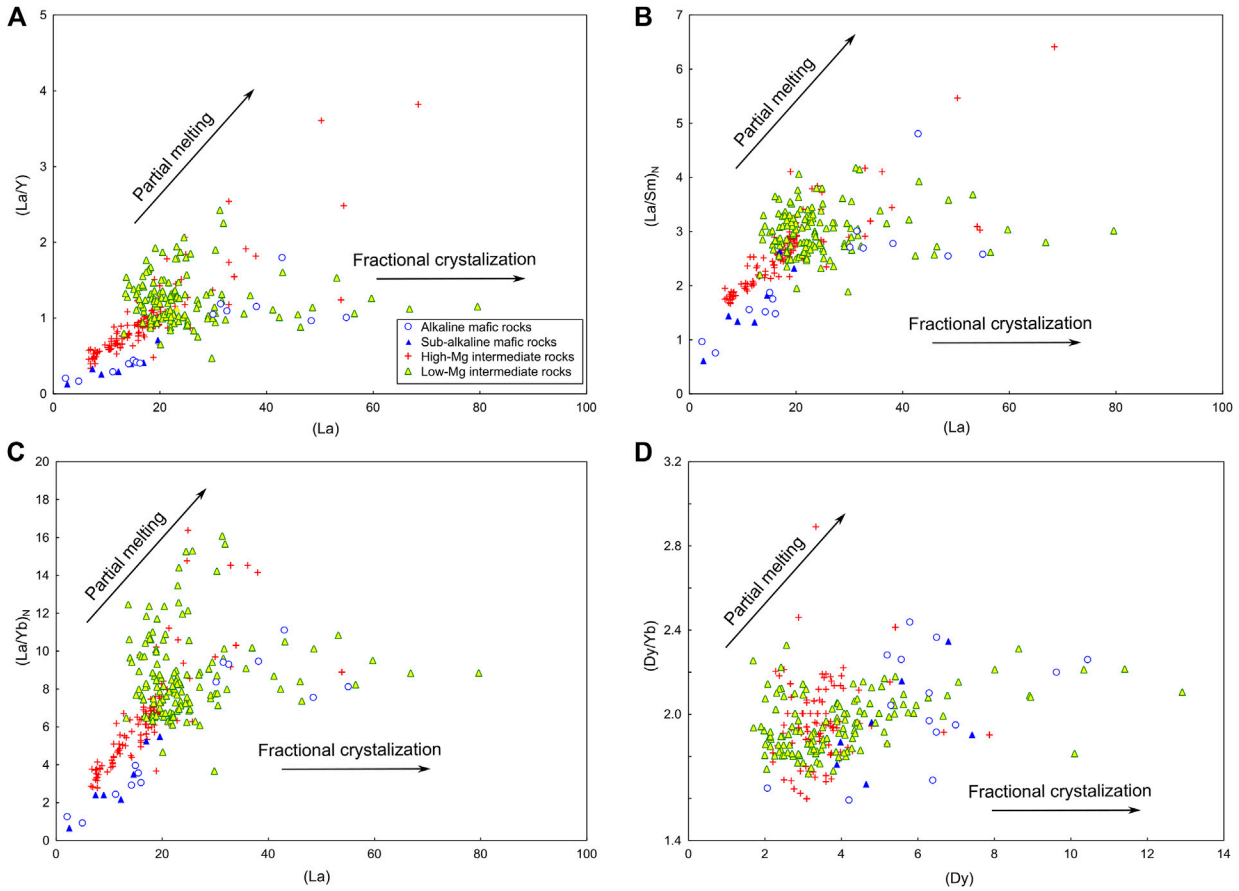

FIGURE 7
(A–D) Immobile trace element ratio diagram illustrating the partial melting and fractionation effects in the MGVF volcanic rocks.

+ 0.02 Sp and 0.63 Ol + 0.30 Opx +0.02 Cpx +0.05 Gt, for garnet-bearing lherzolite melt. Partition coefficients considered for both models were taken from McKenzie and O'Nions (1991). Partial melting models were used for melting degrees of 1–50% (F = 0.01–0.2). Partial melt models (Figure 8) reveal that rocks from the mafic group plot similar REE trends to spinel-bearing lherzolite partial melts (~1–15%), suggesting that these rocks were generated through melting of a spinel-bearing lherzolite mantle source (Figure 8A). Alkaline rocks show similarities with the sub-alkaline rocks and are consistent with low degrees of partial melting in a spinel-bearing lherzolite. Moreover, the composition of some alkaline rocks suggests even higher degrees of partial melting than sub-alkaline rocks; an ongoing research in our group is investigating if this difference could be attributed to more interaction with the upper crust.

These ranges of partial melting are also observed in incompatible trace element ratio models (Figures 8C,D), which suggest that mafic magmas were derived by 5%–15% of partial melting in a spinel-bearing lherzolite. These percentages of melting can be compared with those proposed by Rasoazanamparany et al. (2016), where they mentioned that high-MgO magmas (MgO = >8%; such as most of mafic magmas from the MGVF; Supplementary Table S4) can be generated by ~ 15% partial melting of sediment and hydrous fluid derived from the oceanic crust. As well, these results are comparable and support the approach of the petrogenesis of mafic magmas of the MGVF proposed by Hasenaka and Carmichael, 1987, Luhr et al. (1989), and Gómez-Tuena et al. (2018).

Although a spinel peridotite's origin confirms previous thoughts about the origin of magmas in the MGVF, the occurrence of alkaline rocks and the concentration of mafic rocks at the central portion of the volcanic field are mainly unexplored issues. An ongoing study is investigating the origin of alkaline rocks in the MGVF with detailed bulk and mineral chemistry; however, it seems that the occurrence of mafic rocks within the volcanic field can be explained with petrogenetic and tectonomagmatic relations.

The spatial distribution of these mafic rocks is mainly located in the central portion of the volcanic field (19°–20° latitude along

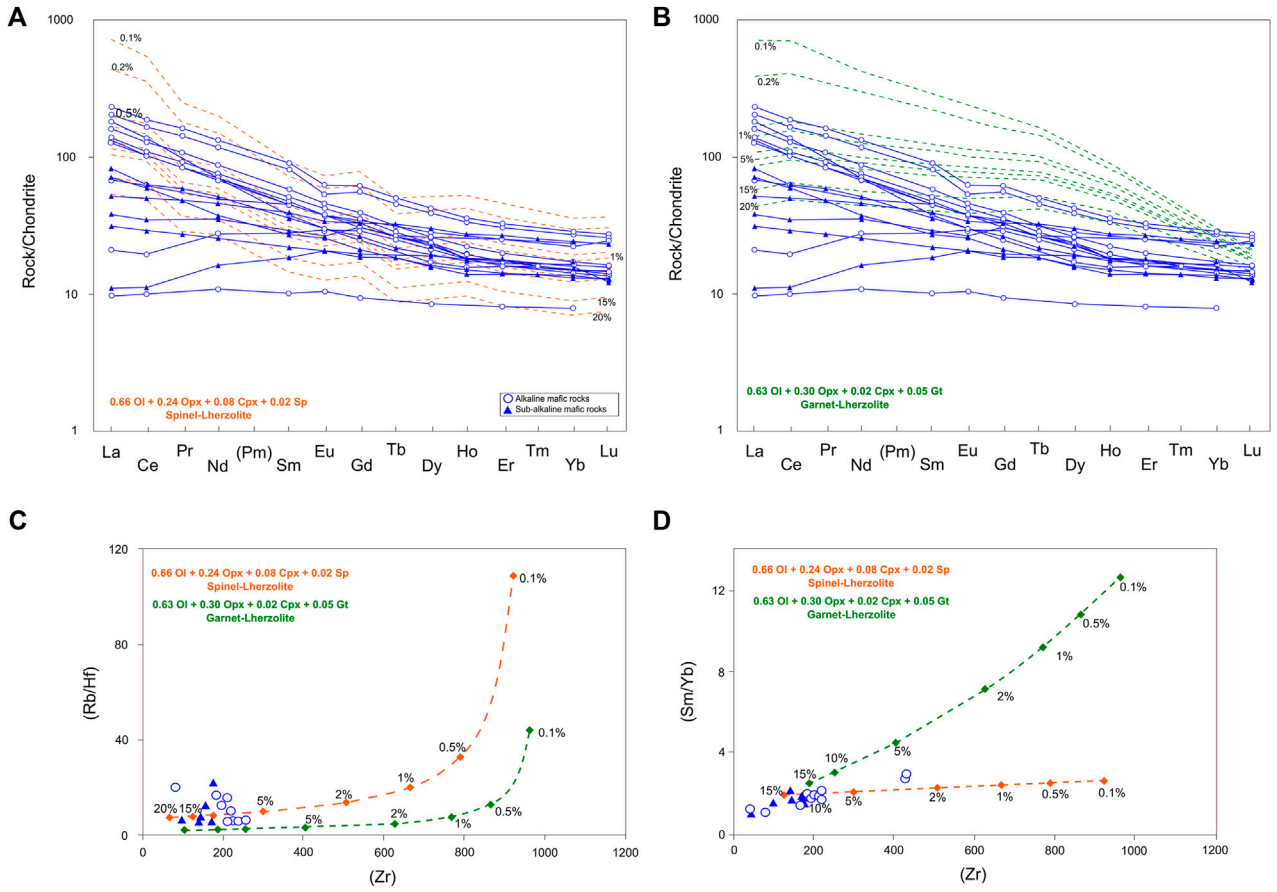

FIGURE 8
(A) Chondrite-normalized partial melt model for mafic magmas from the MGVF showing partial melting curves of spinel-bearing lherzolite melt. **(B)** Chondrite-normalized partial melt model for mafic magmas from the MGVF displaying partial melting curves of garnet-bearing lherzolite melt. Partial melt curves were generated at the degree of melting *F = 0.01–0.2*, applying batch melting equations reported by Zou (2007). More details are given in the text. The chondrite and primitive mantle values from normalization are taken from McDonough and Sun (1995). **(C)** (Zr) vs. (Rb/Hf) bivariate diagram showing partial melt model for mafic magmas from the MGVF. The melting curves are generated at the same degrees of melting *F = 0.01–0.2*. The mineralogical compositions are reported in orange for the spinel-bearing lherzolite curve and green for garnet lherzolite curve. **(D)** (Zr) vs. (Sm/Yb) bivariate diagram showing partial melt model for mafic magmas from the MGVF. Conditions of the model are reported in text.

the longitude 100°–103°; Figure 1B). It has to be noticed that mafic rocks distribution is based in published data that is available until the generation of the present work; hence, the sampling of these rocks is probably biased. Nevertheless, according to Avellán et al. (2020) and Menella et al. (2022), this area is tectonically controlled by the Tarímbaro graben which takes part as one of the 10 fault segments from the Morelia–Acambay Fault system (MAFS; Avellán et al., 2020). The Tarímbaro graben is located to the north of the MAFS and consists of dextral strike-slip faults that affect the NE part of the MGVF, especially at the city of Morelia, producing related normal faults (Figure 1B). (Avellán et al., 2020). The Tarímbaro graben system, compared to other extension areas of the MGVF (e.g., Suter 2016; Avellán et al., 2020), has been proposed to have deeper faults, which affect the whole crust (Avellán et al., 2020; Menella et al., 2022). In addition, mafic volcanism appears in the western segment of Tarímbaro graben. It coincides with the area with highest rate of extension from the region, according to the state of recent deformation through a structural analysis and the regional stress regime from focal mechanisms (Menella et al., 2022). This structural and stress setting together with the low grades of partial melting of spinel-bearing lherzolite is described in Figure 8, which suggest that the origin of these mafic rocks can be the result of a rapid ascent of magmas from the mantle. This rapid ascent can be related with the trend of OIB compositions in immobile trace element (Figure 6) where it marks a primitive source and the flat pattern in chondrite-normalized REE and multielement diagram trends (Figure 4), indicating that these rocks could be derived from subcontinental lithospheric mantle. Thus, it highlights the critical role of local structural settings in controlling the magma ascents and their compositions.

Therefore, we consider the generation and rapid ascent of mafic magmas in the MGVF could not be limited only to the Tarímbaro graben, taking into account the potential lack of available data on mafic rock distributions across the volcanic field. Future studies need to focus on the identification and characterization of mafic rocks on the MGVF.

5.2 Origin of the intermediate magmatism

The intermediate volcanic rocks of the MGVF are dispersed within the 19°68′ to 20°05′ latitude along the longitude 100°27′ to 103°40′ (Figure 1B). Several authors have proposed different origin and evolution processes for the intermediate magmas of the MGVF (e.g., Luhr et al., 1989; Verma and Hasenaka, 2004; Gómez-Vasconcelos et al., 2015; Chevrel et al., 2016; Lossantos et al., 2017). Verma and Hasenaka (2004) proposed that intermediate magmas were formed by a heterogeneous mantle source, likely a veined mantle, and fractional crystallization. On the other hand, Losantos et al. (2017) mentioned that this type of rocks is derived from low degrees of crystallization and contamination with heterogeneous granitic components that involves distinct paragenetic assemblages. In addition, neglecting both mechanisms, Ownby et al. (2011) suggested that andesites within the Tancitaro area are formed by partial melting of hornblende-rich gabronorites.

In addition to the processes accounted for the MGVF, orogenic andesites worldwide have been reported as a product of high-pressure fractionation from a primary hydrous basaltic magma (e.g., Sisson and Grove, 1993; Ownby et al., 2007) or fractionation of olivine and clinopyroxene (low-Mg intermediate rocks; e.g., Smith, 2013). Also, it has been proposed that orogenic andesites can be produced by magma mixing with or without crustal contamination (e.g., Rollinson, 1993; Reubi and Blundy, 2009; Kent et al., 2010; Straub et al., 2011; Gómez-Tuena et al., 2014).

In order to contribute with the knowledge of the genesis of the intermediate magmas from the MGVF, we used a robust dataset formed by published data (n = 407; Supplementary Table S4). We sub-divided all the intermediate rocks into a low-Mg and a high-Mg series and modeled a series of immobile trace elements (Figure 7). According to these models, high-Mg intermediate rocks can be explained with variable degrees of partial melting. We recognized the same could be modeled for the sub-alkaline mafic rocks; thus, in addition to the primary partial melting, another process such as mixing or assimilation must be overprinted (e.g., Losantos et al., 2017). In contrast, low-Mg intermediate rocks are less variable and fall in a constrained compositional range, although aspects of their composition suggest that fractional crystallization dominates their composition (Figure 7). In any case, it seems that such differences are controlled either by heterogeneities in the source rocks or fractionation of different mineral assemblages at variable depths.

Thus, given the different intermediate rock series that occur in the volcanic field (low-Mg and high-Mg), we explored the processes that controlled the final composition of intermediate magmas from the MGVF.

We evaluated first the impact of fractional crystallization. Low-Mg rocks show constant Mg# for variable SiO_2 contents (Figure 9); although high-Mg rocks apparently increase their overall Mg# with SiO_2 increments (Figure 9), the MgO vs. SiO_2 relation is inverse (Figure 9); hence, Mg# could be evaluated to be constant with SiO_2 increment. In order to maintain a constant Mg#, MgO should decrease by fractional crystallization and Fe^{+2} should have subtle decrease. It is well known that crystallization of hydrous basalts stabilizes olivine over pyroxene and that magnetite is a stable phase (e.g., Sisson, 2015); these processes could account for the dominant depletion of MgO over Fe^{+2} required to produce the trends observed in Figure 9.

It is well recognized that low-Mg intermediate magmas could be partial melts of olivine peridotites further modified in arc crust environments (Straub et al., 2014). Although high-Mg intermediate magmas should experience the same physical and thermal barriers as low-Mg magmas during their migration to the surface, their high Ni contents are characteristic; Straub et al. (2014) suggested that this type of rocks were produced by partial melting of pyroxenites, previously formed by mantle peridotites modified by silicic slab components. Figure 9 shows the contrast in Ni content of the intermediate magmas for the MGVF; high-Mg rocks show variable Ni contents and definitely are more enriched in Ni than low-Mg rocks. This reflects mantle heterogeneities below the MGVF with discrete zones of metasomatized mantle. Where and when these magmas reach the surface might depend on the time and space variations of the stress field, similar to the mafic magmas that erupted along the volcanic field. Figure 9 show the Sr–Zr content of low-Mg rocks and high-Mg rocks; both series contain similar concentrations, except for high-Mg rocks which show a low Sr–Zr group of samples. Furthermore, the Ba/Nb vs. Nb diagram from Figure 9F shows that low-Mg and high-Mg intermediate rocks have lower abundances of incompatible trace elements, which could require a more trace element depleted source and/or higher degrees of melting; therefore, it can be suggested that these rocks must be derived from a compositionally different lherzolite or mafic source which can be differentiated by a less enriched lherzolite source or by HFSE-rich basalts (e.g., Wanke et al., 2019). The slight enrichments in LREE and LILE over HREE and HFSE (Figures 7C,D) could argument a subduction component in intermediate rocks genesis (e.g., Wanke et al., 2019b).

As suggested in Sosa-Ceballos et al. (2021), the stress field might play an important role during the assimilation and fractional crystallization processes that modified the composition of intermediate and felsic magmas in the MGVF.

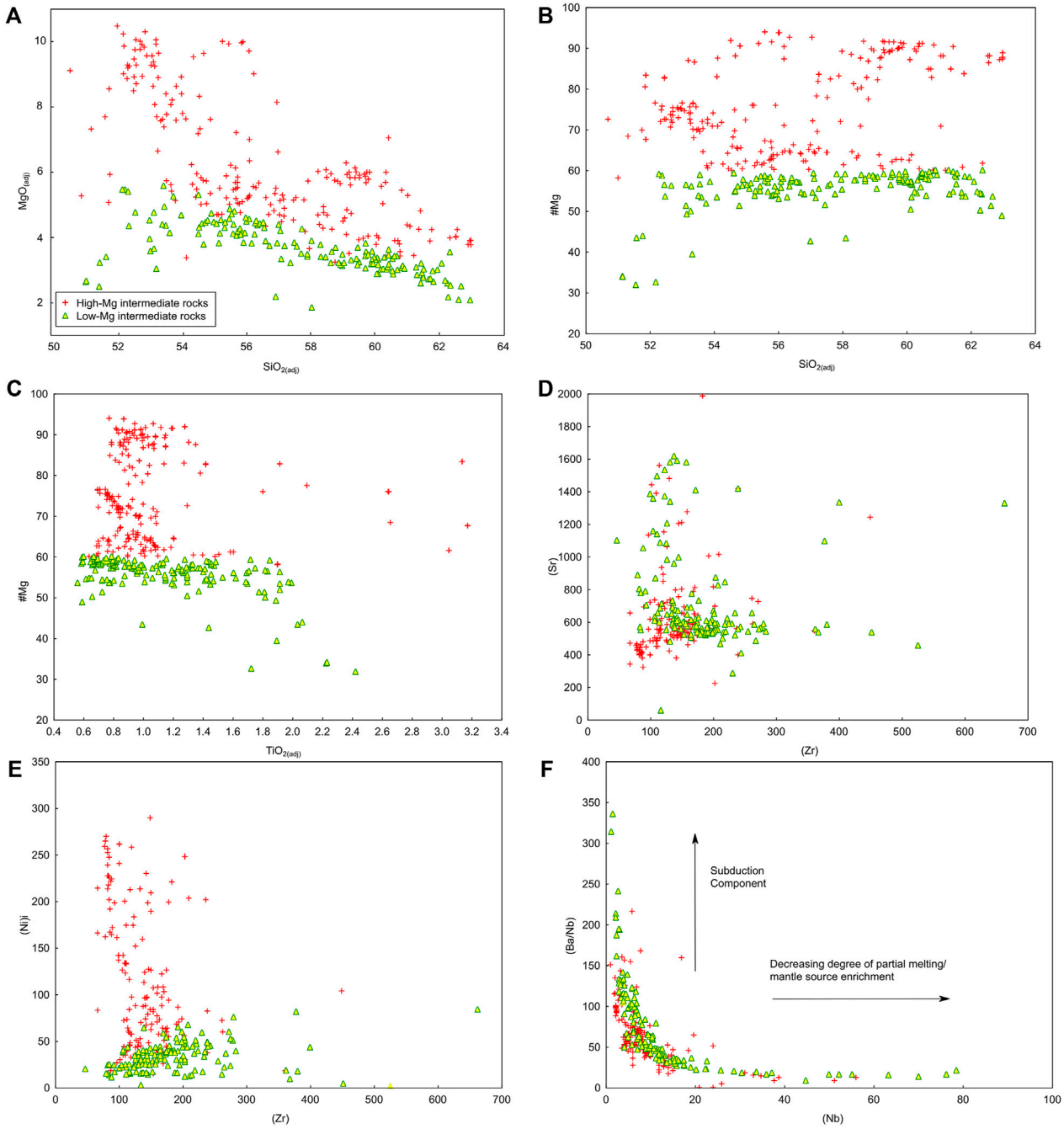

FIGURE 9
(A–F) Bivariate diagrams of major and trace elements for low-Mg and high-Mg intermediate volcanic rocks from the MGVF. The low-Mg intermediate magmas display constant #Mg for variable SiO_2 contents that can suggest crystallization effects. The high Ni contents in high-Mg intermediate magmas suggest mantle heterogeneities below the MGVF with distinct metasomatized mantle areas.

We investigated what type of rocks might modify mafic magmas to produce more evolved rocks. The models comprise three low-crust xenoliths, one from San Luis Potosí (sample LP89 reported by Schaaf et al., 1994) and two found in volcanic rocks from the northern portion of the MGVF (sample JOR0712 reported by Rasoazanamparany et al., 2016 and the VS.1 sample reported by Ortega-Gutiérrez et al., 2014), granites from the Michoacán local basement and alkaline to sub-alkaline volcanic rocks (HM90 sample reported by Lapierre et al., 1992). Binary models show that the compositional variability of the

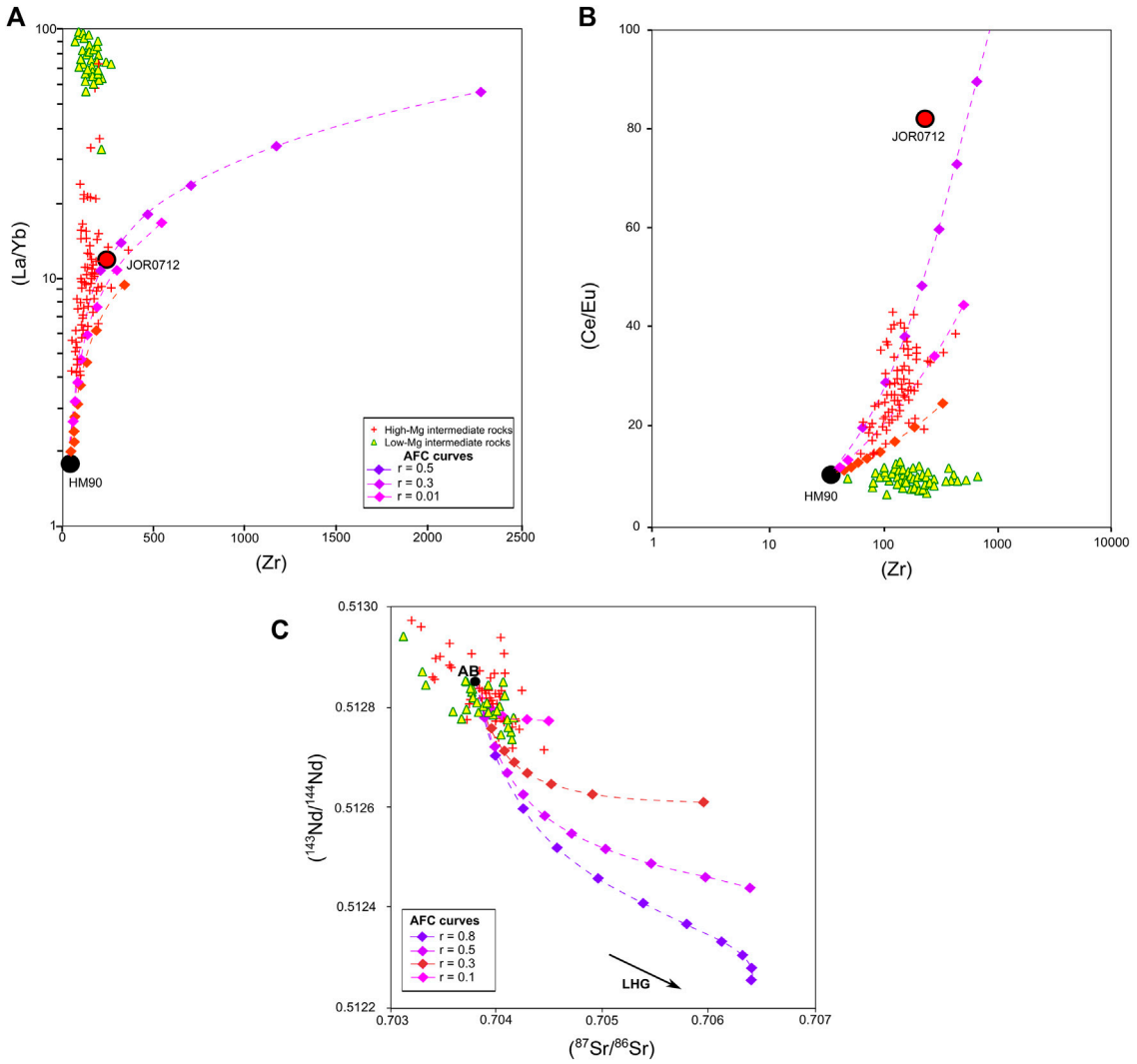

FIGURE 10
(A,B) Bivariate assimilation-fractional crystallization model for intermediate magmas from the MGVF. The intermediate magmas display high ratios of fractional crystallization and low ranges of assimilation between mafic melt (HM90) and granitic component (JOR0712; $r \sim =0.001–0.1$). **(C)** Sr–Nd isotope assimilation and fractional crystallization model for intermediate magmas from the MGVF, which display ratios of assimilation between $r = 0.1$ and $r = 0.3$. The LHG samples were taken from Luhr and Carmichael, (1985b); Luhr, (1997).

intermediate rocks cannot be attained mixing the low-crust and either, alkaline or sub-alkaline magmas (Supplementary Figure S1). Although mixing, or assimilation, of the lower crust does not domain the evolution of the magmas, some fractional crystallization might occurred at lower-crust depth and contribute to the magma evolution. If the low crust is not dominantly involved, we investigated if the upper crust is relatively more integrated in the composition of the intermediate rocks.

We generated a series of AFC models to evaluate this process (Figure 10); we evaluated separately the low- and high-Mg series. These models were generated according to the equation described by De Paolo (1981) using trace element composition of the alkaline basic samples from MGVF (HM90; concentration reported by Lapierre et al., 1992), as initial magma (C_0), and a granitic composition from the MGVF (JOR0712; concentration reported by Rasoazanamparany et al., 2016) as assimilated wall rock (C_A). The mineral arrangement of 0.35 Opx + 0.25 Cpx + 0.1 Ap + 0.3 Plg was considered for a fractional crystallization process based on those proposed by Aguirre-Espinosa et al. (2022) for Sierra de Chichinautzin intermediate volcanic rocks. Partition coefficients were taken from Ersoy and Helvaci (2010). Fractional values of the remaining magma were of 0–0.09, and the ratio of assimilation to fractional crystallization was $r = 0.01$, $r = 0.1$, and $r = 0.5$.

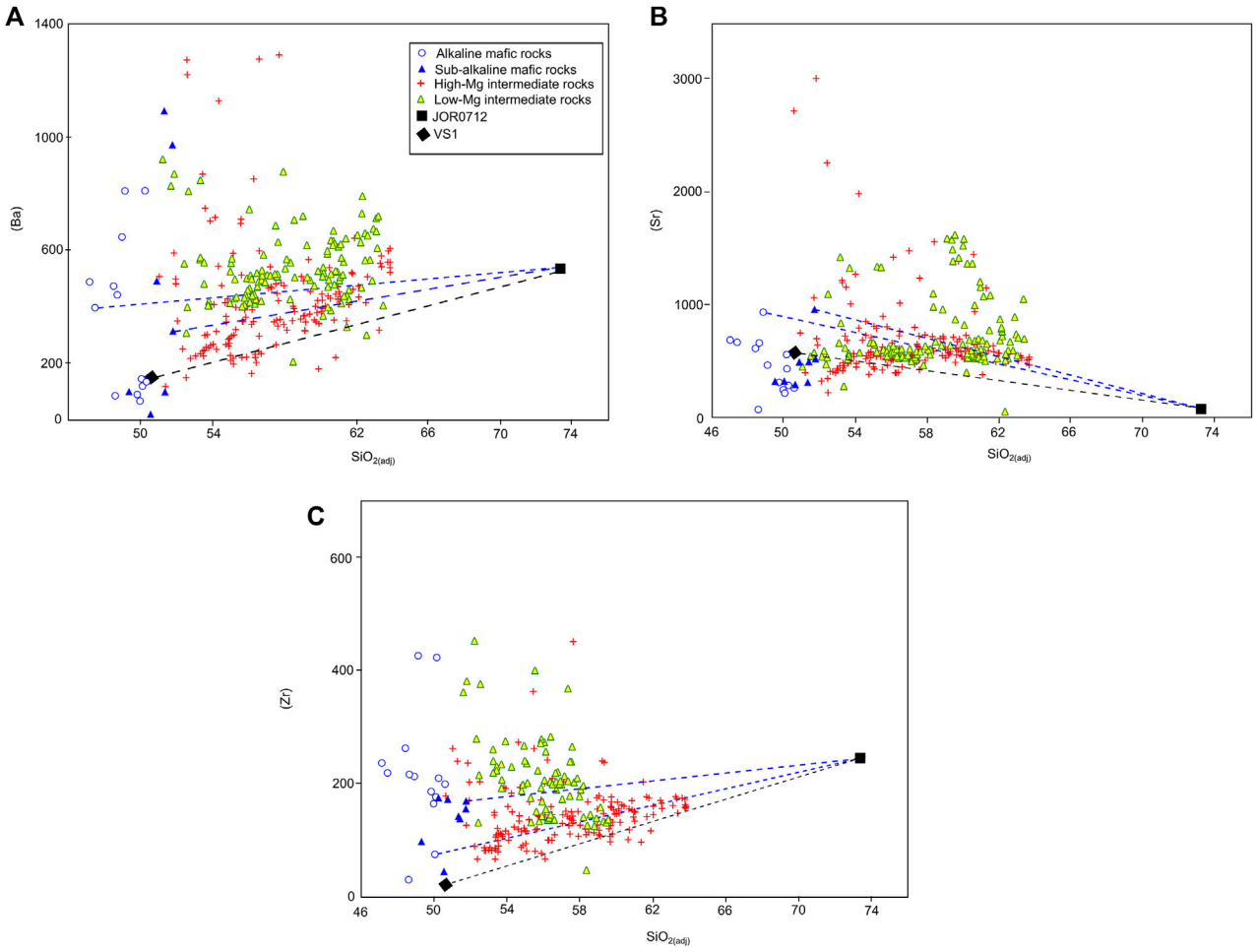

FIGURE 11
(A–C) Bivariate diagrams of SiO_2 vs. trace elements for low-Mg and high-Mg intermediate volcanic rocks from the MGVF. The black line represent mixing curve between granitic end-members. The blue line display mixing curves between alkaline and sub-alkaline with a granitic end-members. Given the overall compositions of mafic rocks, one or multiple mafic melts could be involved. The granitic samples (JOR0712 and VS.1) show a relatively similar trend to intermediate volcanic rocks, suggesting low degrees of assimilation. The low-Mg intermediate rocks display an increase with SiO_2 increments such in Sr and Ba, which suggests fractional crystallization, whereas that in Zr vs. SiO_2 diagram displays a decrease with spread trend with SiO_2 increments. The high-Mg intermediate rocks show a from constant to increase in trace element with the SiO_2 increments, which suggests that fractional crystallization was not dominant; hence, a crustal assimilation could be occurred.

The most striking result is how rocks from the high-Mg series can be explained with variable rates of assimilation and fractional crystallization using an alkaline basalt and La Huacana Granite as end-members (Figure 10), whereas rocks from the low-Mg series are completely unrelated to the model (Figures 10A,B). The mixing between the upper crust and most likely some alkaline basalt could be suggested with the binary diagrams shown in Figure 11.

A complementary model was developed in base of Sr-Nd isotopic composition (Figure 10C). This model was constructed following the same mineral arrangement and partition coefficient of bivariate trace element model, but a different assimilated wall rock have been considered (LHG sample taken from Luhr and Carmichael, 1985b; Luhr 1997) due the scare of isotopic information of the sample used in trace element models. Such as in the AFC bivariate trace element model, the isotopic composition model suggest that intermediate magmas were generated through the fractional crystallization of a mafic parental magma and was contaminated by a granitic crust at low rates of fractional crystallization–assimilation (r = ~ 0.1–0.3).

As already stated for felsic rocks (e.g., Sosa-Ceballos et al., 2021), tectonic stresses might define the evolution and final composition of intermediate rocks. We suggest that high-silica intermediate rocks represent magmas that were trapped in compressional zones and hosted by granites for

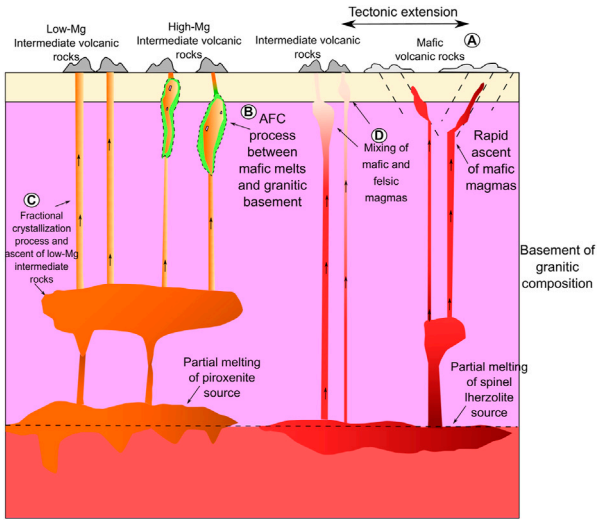

FIGURE 12
Schematic model for the evolution of the mafic and intermediate magmas from the MGVF. **(A)** Mafic rocks were generated through partial melting of lherzolite sources and display a rapid ascent from the asthenosphere to the surface, which is related to local extensional stresses. **(B)** Assimilation and fractional crystallization (AFC) processes show an important role in final composition of high-Mg rocks (green patch). **(C)** Fractional crystallization and/or partial melting of heterogeneous sources (e.g., piroxenites) that contributed to low–high Mg content before intermediate melts arrived to the upper crust. **(D)** Mixing of mafic and felsic magmas in shallow levels of the continental crust; felsic magmas were produced by partial melting of the local basement (modified from Sosa-Ceballos et al., 2021).

longer periods of time, whereas low-silica intermediate rocks represent magmas more easily tapped to the surface. Because both type of rocks commonly contain quartz xenocrysts (e.g., Suhardja et al., 2015; Osorio-Ocampo et al., 2018; Pérez-Osorio et al., 2018; Ramírez and Uribe, 2019; Reyes-Guzmán et al., 2021), to investigate which type of intermediate rock (low-Mg and high-Mg) contain greater contents of quartz and relate their abundance to their relative residence time in the upper crust is a pending task.

Even the AFC models suggest that the high-Mg intermediate rocks are influenced by the assimilation of granites, we recognize the models are subjugated to uncertainties derived from the distribution coefficients of the chosen elements, the chosen mineral assemblages and the fact that the only driving force accounted is the latent heat of crystallization (underestimating heating processes by other magmas). Hence, which other processes could account for magma intermediate compositions? We previously suggested that more mafic rocks in the MGVF reflect mantle heterogeneities. In addition, the intermediate rocks are consistent, at least partially, with a flux melting model, in which the addition of volatiles encourages higher extents of melting and the development of wet magmas with higher LILE/HFSE ratios (Diaz-Bravo et al., 2014). This flux model is mainly based in the hypothesis that hydrous slab contributions are usually small, and consequently unable to exert a significant petrologic transformation of the mantle wedge below arcs (Díaz-Bravo et al., 2014). However, Grove et al. (2012) have mentioned that water and other volatiles play an important role in the melting behavior of peridotite at subduction zones, and that water is not the only component being transferred to the mantle wedge at convergent margins (e.g., Díaz-Bravo et al., 2014). As diverse authors have proposed (e.g. Gómez-Tuena et al., 2007; CooperRuscitto et al., 2012; Díaz-Bravo et al., 2014), melts from recycled sediments, subducted basalts and eroded crust can contribute significant amounts of silica to the mantle, and this can act as an effective metasomatic agent than solute-poor hydrous fluids, as well, if contribution of recycled silica is significant, the source of arc magmas will no longer be peridotitic, and the melting products will gradually become more intermediate.

Overall, intermediate rocks from the MGVF show variable Pb and Zr contents for a given SiO_2 value (Supplementary Figure S2); at first glance this suggests that slab fluids were involved in the process and that heterogeneous domains of the mantle wedge were melted to produce the chemical diversity of the rocks observed. But as shown before, the presence of xenocrysts and the tectonomagmatic relations of felsic and intermediate rocks in the MGVF suggest that the integrated composition of intermediate rocks reflect a diversity of processes, very difficult to quantify.

Hence, we cannot neglect the fact that magmas arrived to the upper crust partially evolved or already formed as andesitic melts by partial melting of the mantle (e.g., Ownby et al., 2011; Sisson, 2015). Moreover, given the low abundance of felsic rocks in the MGVF, we cannot neglect the possibility that intermediate rocks are a mixture of mafic and felsic magmas (e.g., Reubi and Blundy 2009). If felsic magmas are produced by partial melting of the local granites (e.g., Sosa-Ceballos et al., 2021) we do not know the rate at which these magmas are produced, thus, perhaps these felsic magmas mixed with more mafic melts and contributed to the generation of intermediate rocks.

6. Conclusion

To summarize our proposal for the generation of mafic and intermediate magmas in the MGVF, a schematic model has been developed (Figure 12). Based on geochemical models, we suggest that mafic magmas are generated through low partial melting grades (~1–15%) of a spinel-bearing lherzolite source. These magmas can be the result of partial melting of a heterogeneous mantle and a rapid ascent from the asthenosphere that is related to the local extensional stress regime that affects the central portion of the MGVF.

On the other hand, intermediate magmas display a more complex petrogenetic story. The analyzed datasets suggest that intermediate rocks can be separated into low-Mg and high-Mg series. Low-Mg intermediate magmas display an obvious impact of fractional crystallization processes. However, the AFC models do not display an obvious control on the generation of low-Mg intermediate rocks; nevertheless, some fractional crystallization might occur along the crust. In addition, AFC models and bivariate trace element ratios suggest that intermediate rocks from the MGVF are affected by mantle heterogeneities that domain the mantle wedge and produce a diverse set of intermediate rocks. This study highlights the necessity to focus on future studies with a regional point of view for a better understanding of the geodynamic and tectonic role that may control the variability of rock composition across the volcanic field.

Author contributions

DT-S, GS-C, XB, and JM contributed to the conception and design of the present work. All authors have contributed to the manuscript revision, edition, and modification through several drafts, and all authors approved the submitted version.

Funding

This study was funded by the project CONACYT-FC2406.

Acknowledgments

DT-S acknowledges the National Council of Science and Technology (CONACYT), Mexico for a postdoctoral fellowship by the project CONACYT-FC2406 (JM) and DGAPA-UNAM.

Conflict of interest

The authors declare that the research was conducted in the absence of any commercial or financial relationships that could be construed as a potential conflict of interest.

Publisher's note

All claims expressed in this article are solely those of the authors and do not necessarily represent those of their affiliated organizations, or those of the publisher, the editors, and the reviewers. Any product that may be evaluated in this article, or claim that may be made by its manufacturer, is not guaranteed or endorsed by the publisher.

Supplementary material

The Supplementary Material for this article can be found online at: https://www.frontiersin.org/articles/10.3389/feart.2022.932588/full#supplementary-material

References

Agrawal, S., Guevara, M., and Verma, S. P. (2008). Tectonic discrimination of basic and ultrabasic volcanic rocks through log-transformed ratios of immobile trace elements. *Int. Geol. Rev.* 50 (12), 1057–1079. doi:10.2747/0020-6814.50.12.1057

Aguirre-Espinosa, J., Velasco-Tapia, F., Rodríguez-Saavedra, P., and Salinas-Jasso, J. A. (2022). "Geochemometrics: Petrology of quaternary volcanism in the central Mexican volcanic belt," in *Geochemical treasures and petrogenetic processes (dedicated to professor surendra P. Verma)*. Editors S. Jhon, P. Kailasa, and S. Verma (Singapore: Springer Nature). in press.

Alanis-Alvarez, S., Nieto-Samaniego, A., Morán-Zenteno, D., and Alba-Aldave, L. (2002). Rhyolitic volcanism in extensión zone associated with strike-slip tectonics in the Taxco región, Southern México. *J. Volcanol. Geotherm. Res.* 118, 1–14. doi:10.1016/s0377-0273(02)00247-0

Anderson, A. T. (1974). Chlorine, sulfur, and water in magmas and oceans. *Geol. Soc. Am. Bull.* 85, 1485–1492. doi:10.1130/0016-7606(1974)85<1485:csawim>2.0.co;2

Avellán, D. R., Cisneros-Máximo, G., Macías, J. L., Gómez-Vasconcelos, M. G., Layer, P. W., Sosa-Ceballos, G., et al. (2020). Eruptive chronology of monogenetic volcanoes northwestern of Morelia-Insights into volcano-tectonic interactions in the central-eastern Michoacán-Guanajuato Volcanic Field. *México. Jou. So. Am. Bull. Sci.* 100, 102554. doi:10.1016/j.jsames.2020.102554

Ban, M., Hasenaka, T., Delgado Granados, H., and Takaoka, N. (1992). K-Ar ages of lavas from shield volcanoes in the Michoacán-Guanajuato volcanic field, Mexico. *Geofísico Int.* 31, 467–473.

Blatter, D. L., Carmichael, I. S. E., Deino, A. L., and Renne, P. R. (2001). Neogene volcanism at the front of the central Mexican volcanic belt: Basaltic andesites to dacites, with contemporaneous shoshonites and high-TiO_2 lava. *Geol. Soc. Am. Bull.* 133, 1324–1342. doi:10.1130/0016-7606(2001)113<1324:nvatfo>2.0.co;2

Blatter, D. L., and Hammersley, L. (2010). Impact of the orozco fracture zone on the central Mexican volcanic belt. *J. Volcanol. Geotherm. Res.* 197, 67–84. doi:10.1016/j.jvolgeores.2009.08.002

Bolós, X., Delgado-Torres, A., Cifuentes, G., Macías, J. L., Bojiseauneau-López, M., Tinoco, C., et al. (2020). Internal structure and hydrothermal fluid circulation of Paricutín volcano, Mexico: Insights gained from near-surface geophysics. *Geophys. Res. Lett.* 47, e2020GL089270. doi:10.1029/2020gl089270

Bolós, X., Macías, J. L., Ocampo-Díaz, Y. Z., and Timoco, C. (2021). Implications of reworking processes on tephra distribution during volcanic eruptions: The case of Paricutín (1943-1952, western Mexico). *Earth Surf. Process. Landf.* 46, 3143–3157. doi:10.1002/esp.5222

Bolós, X., Marti, J., Becerril, I., Grosse, P., Planagumá, I., and Barde-Cabusson, S. (2015). Volcano-structural analysis of La garrotxa volcanic field (NE iberia): Implications for the plumbing system. *Tectonophysics* 642, 58–70. doi:10.1016/j.tecto.2014.12.013

Carmichael, I. S. E., Frey, H. M., Lange, R. A., and Hall, C. M. (2006). The Pleistocene cinder cones surrounding Volca´n colima, Mexico re-visited: Eruption ages and volumes, oxidation states, and sulfur content. *Bull. Volcanol.* 68, 407–419. doi:10.1007/s00445-005-0015-8

Carrasco-Nuñez, G., Righter, K., Chesley, J., Siebert, L., and Aranda-Gómez, J. J. (2005). Contemporaneous eruption of calc-alkaline and alkaline lavas in a continental arc (eastern Mexican volcanic belt): Chemically heterogeneous but isottopically homogeneous source. *Contrib. Min. Pet.* 150, 423–440. doi:10.1007/s00410-005-0015-x

Cébria, J. M., Martiny, B. M., López-Ruiz, J., and Morán-Zenteno, D. J. (2011). The parícutín calc-alkaline lavas: New geochemical and petrogenetic modelling constraints on the cristal assimilation process. *J. Vol. Geo. Res.* 201, 113–125. doi:10.1016/j.jvolgeores.2010.11.011

Chesley, J., Ruiz, J., Righter, K., Ferrari, L., and Gómez-Tuena, A. (2002). Source contamination versus assimilation: An example from the Trans-Mexican Volcanic Arc. *Earth Planet. Sci. Lett.* 195, 211–221. doi:10.1016/s0012-821x(01)00580-5

Chevrel, M. O., Guilbaud, M. N., and Siebe, C. (2016). The ~ AD 1250 effusive eruption of el metate shield volcano (Michoacán, Mexico): Magma source, crustal storage, eruptive dynamics, and lava rheology. *Bull* 78, 1–28. doi:10.1007/s00445-016-1020-9

Cooper, L. B., Ruscitto, D. M., Plank, T., Wallace, P. J., Syracuse, E. M., and Manning, C. E. (2012). Global variations in H_2O/Ce: 1 slab surface temperatures beneath volcanic arcs. *Geochem. Geophys. Geosyst.* 13. doi:10.1029/2011gc003902

Corona-Chávez, P., Reyes-Salas, M., Garduño-Monroy, V. H., Israde-Alcántara, I., Lozano Santa Cruz, R., Morton-Bernea, O., et al. (2006). Asimilación de xenolitos graníticos en el Campo volcánico michoacán-guanajuato: EL caso de Arócutín Michoacán. *México. Rev. Mex. Cie. Geo.* 23, 233–245.

de Cserna, Z. (1971). Precambrian sedimentation, tectonics, and magmatism in Mexico. *Geol. Rundsch.* 60, 1488–1513. doi:10.1007/bf02132764

De Paolo, D. J. (1981). Trace element and isotopic effects of combined wallrock assimilation and Fractional crystallization. *Earth Planet. Sci. Lett.* 53, 189–202. doi:10.1016/0012-821x(81)90153-9

Defant, M. J., Richerson, P. M., De Boer, J. Z., Stewart, R. H., Maury, R. C., Bellon, H., et al. (1991). Dacite genesis via both slab melting and differentiation: Petrogenesis of La Yeguada volcanic complex, Panama. *J. Petrology* 32, 1101–1142. doi:10.1093/petrology/32.6.1101

Demant, A. (1978). Características del Eje Neovolcánico Transmexicano y sus problemas de interpretación. *Univ. Nac. Autónoma México, Inst. Geol. Rev. Mex. Ciencias Geol.* 2, 172–187.

Díaz-Bravo, B. A., Gómez-Tuena, A., Ortega-Obregón, C., and Pérez-Arvizu, O. (2014). The origin of intraplate magmatism in the western Trans-Mexican Volcanic Belt. *Geosphere* 10, 340–373. doi:10.1130/ges00976.1

Drummond, M. S., and Defant, M. J. (1990). A model for trondhjemite-tonalite-dacite genesis and crustal growth via slab melting: Archean to modern comparisons. *J. Geophys. Res.* 95, 21503–21521. doi:10.1029/jb095ib13p21503

Ersoy, Y., and Helvaci, C. (2010). FC–AFC–FCA and mixing modeler: A Microsoft® Excel© spreadsheet program for modeling geochemical differentiation of magma by crystal fractionation, crustal assimilation and mixing. *Comput. Geosci.* 36, 383–390. doi:10.1016/j.cageo.2009.06.007

Ferrari, L., Orozco-Esquivel, T., and Manea, M. (2012). The dynamic history of the Trans-Mexican Volcanic Belt and the Mexico subduction zone. *Tectonophysics* 522-523, 122–149. doi:10.1016/j.tecto.2011.09.018

Ferrari, L., Petrone, C. M., and Francalanci, L. (2002). Reply: "Generation of ocean-island basalt type volcanism in the western Trans-Mexican volcanic belt by slab rollback, asthenosphere infiltration, and variable flux melting. *Geol.* 114, 858–859. doi:10.1130/0091-7613(2002)030<0858:>2.0.co;2

Ferrari, L., Rosas-Elguera, J., Marquez, A., Oyarzun, R., Doblas, M., and Verma, S. P. (1999). Alkaline (ocean-island basalt type) and calc-alkaline volcanism in the Mexican volcanic belt: A case for plume-related magmatism and propagating rifting at an active margin? *Geol.* 27, 1055–1056. doi:10.1130/0091-7613(1999)027<1055:aoibta>2.3.co;2

Ferrari, L. (2004). Slab detachment control on mafic volcanic pulse and mantle heterogeneity in central Mexico. *Geol.* 32, 77–80. doi:10.1130/g19887.1

Fisk, M. R. (1986). Basalt magma interaction with harzburgite and the formation of high-magnesium andesites. *Geophys. Res. Lett.* 13, 467–470. doi:10.1029/gl013i005p00467

Foshang, W. F., and González, R. J. (1956). Birth and development of paricutín volcano, Mexico. *Geo. Su. Bull.* 965-D, 355–489.

Frey, F. A. (1980). The origin of pyroxenites and garnet pyroxenites from Salt Lake Crater, Oahu, Hawaii: Trace element evidence. *Am. J. Sci.* 280A, 427–444.

Freydier, C., Lapierre, H., Ruiz, J., Tardy, M., Martinez-R, J., and Coulon, C. (2000). The early cretaceous arperos basin: An oceanic domain dividing the guerrero arc from nuclear Mexico evidenced by the geochemistry of the lavas and sediments. *J. South Am. Earth Sci.* 13, 325–336. doi:10.1016/s0895-9811(00)00027-4

Gao, R., Xiao, L., Pirajno, F., Wang, G. C., He, X. X., Yang, G., et al. (2014). Carboniferous–permian extensive magmatism in the west junggar, xinjiang, northwestern China: Its geochemistry, geochronology, and petrogenesis. *Lithos* 204, 125–143. doi:10.1016/j.lithos.2014.05.028

Garduño-Monroy, V. H., Chávez-Hernández, J., Aguirre-González, J., Vázquez-Rosas, R., Mijares-Arellano, H., Israde-Alcántara, I., et al. (2009). Zonificación de los periodos naturales de oscilación superficia en la ciudad de Pátzcuaro, Mich., México, con base en microtremores y estudios de paleosismología. *Rev. Mex. Cienc. Geol.* 26, 623–637.

Gómez-Tuena, A., LaGatta, A. B., Langmuir, C. H., Goldstein, S. L., Ortega-Gutiérrez, F., and Carrasco-Nuñez, G. (2003). Temporal control of subduction magmatism in the eastern Trans-Mexican volcanic belt: Mantle sources, slab contributions, and cristal contamination. *Geochem. Geophys. Geosystems* 4, 8912. doi:10.1029/2003GC000524

Gómez-Tuena, A., Mori, L., and Straub, S. M. (2018). Geochemical and petrological insights into the tectonic origin of the Transmexican Volcanic Belt. *Earth-science Rev.* 183, 153–181. doi:10.1016/j.earscirev.2016.12.006

Gómez-Tuena, A., Orozco-Esquivel, M., and Ferrari, L. (2005). Petrogénesis ígnea de la faja volcánica transmexicana. *Bol. Soc. Geol. Mex.* 57 (3), 227–283. doi:10.18268/bsgm2005v57n3a2

Gómez-Tuena, A., Orozco-Esquivel, M. T., and Ferrari, L. (2007). "Igneous petrogenesis of the Trans-Mexican volcanic belt," in *Geology of Mexico: Celebrating the centenary of the*. Editors S. A. Alaniz-Álvarez and A. F. Nieto-Samanieto (Colorado, USA: Geological Society of America), 129–181.

Gómez-Vasconcelos, M. G., Garduño-Monroy, V. H., Macías, J. L., Layer, P. W., and Benowitz, J. A. (2015). The Sierra de Mil cumbres, michoacán-méxico: Transitional volcanism between the Sierra madre Occidental and the Trans-Mexican volcanic belt. *J. Volcanol. Geotherm. Res.* 301, 128–147. doi:10.1016/j.jvolgeores.2015.05.005

Gómez-Vasconcelos, M. G., Macías, J. L., Avellán, D. R., Sosa-Ceballos, G., Garduño-Monroy, V. H., Cisneros-Máximo, G., et al. (2020). The control of preexisting faults on the distribution, morphology, and volume of monogenetic volcanism in the Michoacán-Guanajuato Volcanic Field. *GSA Bull.* 132 (11-12), 2455–2474. doi:10.1130/b35397.1

Grove, T. L., Till, C. B., and Krawczynski, M. J. (2012). The role of H_2O in subduction zone magmatism. *Annu. Rev. Earth Planet. Sci.* 40, 413–439. doi:10.1146/annurev-earth-042711-105310

Guilbaud, M. N., Siebe, C., Layer, P., Salinas, S., Castro-Govera, R., Garduño-Monroy, V. H., et al. (2011). Geology, geochronology, and tectonic setting of the Jorullo volcano región, Michoacán, México. *J. Volcanol. Geotherm. Res.* 201, 97–112. doi:10.1016/j.jvolgeores.2010.09.005

Guilbaud, M. N., Siebe, C., Layer, P., and Salinas, S. (2012). Reconstruction of the volcanic history of the Tacámbaro-Puruarán area (Michoacán, México) reveals high frequency of Holocene monogenetic eruptions. *Bull. Volcanol.* 74, 1187–1211. doi:10.1007/s00445-012-0594-0

Guilbaud, M. N., Siebe, C., Rasoazanamparany, C., Widom, E., Salinas, S., and Castro-Govea, R. (2019). Petrographic, geochemical and isotopic (Sr-Nd-Pb-Os) study of plio-quaternary volcanics and the tertiarybasement in the jorullo-tacámbaro area, michoacán-guanajuato volcanic field, Mexico. *J. Petrology* 60, 2317–2338. doi:10.1093/petrology/egaa006

Hasenaka, T., and Carmichael, I. S. E. (1985). The cinder cones of Michoacán-Guanajuato, Central Mexico: Their age, volume and distribution, and magma discharge rate. *J. Volcanol. Geotherm. Res.* 25, 105–124. doi:10.1016/0377-0273(85)90007-1

Hasenaka, T., and Carmichael, I. S. E. (1987). The cinder cones of michoac n-guanajuato, Central Mexico: Petrology and chemistry. *J. Petrology* 28, 241–269. doi:10.1093/petrology/28.2.241

Hasenaka, T. (1994). Size, distribution, and magma output rate for shield volcanoes of the Michoacán-Guanajuato volcanic field, Central Mexico. *J. Volcanol. Geotherm. Res.* 63, 13–31. doi:10.1016/0377-0273(94)90016-7

Hawkesworth, C. J., Hergt, J. M., Ellam, R. M., and McDermott, F. (1991). Element fluxes associated with subduction related magmatism. *Phil. Trans. R. Soc. Lond.* 335, 393–405. doi:10.1098/rsta.1991.0054

Hernández-Bernal, M. S., Corona-Chávez, P., Solís-Pichardo, G., Schaaf, P., Solé-Viñas, J., and Molina, J. F. (2016). Miocene andesitic lavas of Sierra de Angangueo: A petrological, geochemical, and geochronological approach to arc magmatism in Central Mexico. *Int. Geol. Rev.* 58, 603–625. doi:10.1080/00206814.2015.1101356

Irvine, T. N., and Baragar, W. R. A. (1971). A guide to the chemical classification of the common volcanic rocks. *Can. J. Earth Sci.* 8, 523–548. doi:10.1139/e71-055

Johnson, C. A., and Harrison, C. G. A. (1990). Neotectonics in central Mexico. *Phys. Earth Planet. Interiors* 64, 187–210. doi:10.1016/0031-9201(90)90037-x

Johnson, C. A., and Harrison, C. G. A. (1989). Tectonics and volcanism in central Mexico: A landsat thematic mapper perspective. *Remote Sens. Environ.* 28, 273–286. doi:10.1016/0034-4257(89)90119-3

Johnson, E. R., Wallace, P. J., Cashman, K. V., Granados, H. D., and Kent, A. J. (2008). Magmatic volatile contents and degassing-induced crystallization at Volcán Jorullo, Mexico: Implications for melt evolution and the plumbing systems of monogenetic volcanoes. *Earth Planet. Sci. Lett.* 269, 478–487. doi:10.1016/j.epsl.2008.03.004

Kelemen, P. B. (1995). Genesis of high Mg# andesites and the continental crust. *Contr. Mineral. Pet.* 120, 1–19. doi:10.1007/bf00311004

Kent, A. J. R., Darr, C., Koleszar, A. M., Salisbury, M. J., and Cooper, K. M. (2010). Preferential eruption of andesitic magmas through recharge filtering. *Nat. Geosci.* 3, 631–636. doi:10.1038/ngeo924

Kim, W. H., Clayton, R. W., and Keppie, F. (2011). Evidence of a collision between the yucatán block and Mexico in the Miocene. *Geophys. J. Int.* 187, 989–1000. doi:10.1111/j.1365-246x.2011.05191.x

Kshirsagar, P., Siebe, C., Guilbaud, M. N., and Salinas, S. (2016). Geological and environmental controls on the change of eruptive style (phreatomagmatic to Strombolian-effusive) of Late Pleistocene El Caracol tuff cone and its comparison with adjacent volcanoes around the Zacapu basin (Michoacán, México). *J. Volcanol. Geotherm. Res.* 318, 114–133. doi:10.1016/j.jvolgeores.2016.03.015

Kshirsagar, P., Siebe, C., Guilbaud, M. N., Salinas, S., and Layer, P. W. (2015). Late Pleistocene Alberca de Guadalupe maar volcano (Zacapu basin, Michoacán): Stratigraphy, tectonic setting, and paleo-hydrogeological environment. *J. Volcanol. Geotherm. Res.* 304, 214–236. doi:10.1016/j.jvolgeores.2015.09.003

La Fléche, M. R., Camire, G., and Jenner, G. A. (1998). Geochemistry of post-acadian, carboniferous continental intraplate basalts from the maritimes basin, magdalen islands, quebec, Canada. *Chem. Geol.* 148, 115–136. doi:10.1016/s0009-2541(98)00002-3

Lapierre, H., Ortiz, L. E., Abouchami, W., Monod, O., Coulon, C., and Zimmermann, J. L. (1992). A crustal section of an intra-oceanic island arc: The Late Jurassic-Early Cretaceous Guanajuato magmatic sequence, central Mexico. *Earth Planet. Sci. Lett.* 108, 61–77. doi:10.1016/0012-821x(92)90060-9

Larrea, P., Albert, H., Ubide, T., Costa, F., Colás, V., Widom, E., et al. (2021). From explosive vent opening to effusive outpouring: Mineral constraints on magma dynamics and timescales at Paricutin monogenetic volcano. *J. Petrology* 62, 1. egaa112. doi:10.1093/petrology/egaa112

Larrea, P., Salinas, S., Widom, E., Siebe, C., and Abbit, R. J. F. (2017). Compositional and volumetric development of a monogenetic lava flow field: The historical case of Paricutin (Michoacán, Mexico). *J. Volcanol. Geotherm. Res.* 348, 36–48. doi:10.1016/j.jvolgeores.2017.10.016

Larrea, P., Widom, E., Siebe, C., Salinas, S., and Kuentz, D. (2019). A re-interpretation of the petrogenesis of Paricutin volcano: Distinguishing crustal contamination from mantle heterogeneity. *Chem. Geol.* 504, 66–82. doi:10.1016/j.chemgeo.2018.10.026

Lassiter, J. C., and Luhr, J. F. (2001). Osmium abundance and isotope variations in mafic Mexican volcanic rocks: Evidence for crustal contamination and constraints on the geochemical behavior of osmium during partial melting and fractional crystallization. *Geochem. Geophys. Geosyst.* 2, 1027. doi:10.1029/2000gc000116

Le Bas, M. J., Le Maitre, R. W., Streckeisen, A., and Zanettin, B. (1986). A chemical classification of volcanic rocks based on the total alkali-silica diagram. *J. Petrology* 27, 745–750. doi:10.1093/petrology/27.3.745

Le Maitre, R. W., Streckeisen, A., Zanettin, B., Le Bas, M. J., Bonin, B., Bateman, P., et al. (2002). *Igneous rocks. A classification and glossary of terms: Recommendations of the international union of geological sciences subcomission of the systematics of igneous rocks*. Cambridge, UK: Cambridge University Press.

Losantos, E., Cebriá, J. M., Morán-Zenteno, D. J., Martiny, B. M., and López-Ruiz, J. (2015). "Composición isotópica de oxigeno de las lavas del volcán Parícutin (Campo volcánico de Michoacán-Guanajuato, México)," in GEOS. Presented at the Reunión Anual de la Unión Geofísica Mexicana, Puerto Vallarta, México, 2-7 November, 98–99.

Losantos, E., Cebriá, J. M., Morán-Zenteno, D. J., Martiny, B. M., and López-Ruiz, J. (2014). Condiciones de cristalización y diferenciación de las lavas del volcán El Metate (Campo Volcánico de Michoacán-Guanajuato, México). *Estud. Geol.* 70, e020. doi:10.3989/egeol.41806.349

Losantos, E., Cebriá, J. M., Morán-Zenteno, D. J., Martiny, B. M., López-Ruiz, J., and Solís-Pichardo, G. (2017). Petrogenesis of the alkaline and calcalkaline monogenetic volcanism in the northern sector of the Michoacán-Guanajuato Volcanic Field (Central Mexico). *Lithos* 288-289, 295–310. doi:10.1016/j.lithos.2017.07.013

Luhr, J. F., Allan, J. F., Carmichael, I. S. E., Nelson, S. A., and Hasenaka, T. (1989). Primitive calc-alkaline and alkaline rock types from the western Mexican Volcanic Belt. *J. Geophys. Res.* 94, 4515–4530. doi:10.1029/jb094ib04p04515

Luhr, J. F., and Carmichael, I. S. E. (1985b). Jorullo Volcano, Michoacán, Mexico (1759-1774): The earliest stages of fractionation in calc-alkaline magmas. *Contr. Mineral. Pet.* 90, 142–161. doi:10.1007/bf00378256

Luhr, J. F., and Lazaar, P. (1985a). The southern Guadalajara volcanic chain, Jalisco, Mexico. *Geof. Int.* 24, 691–700.

Mahgoub, A. N., Böhnel, H., Siebe, C., Salinas, S., and Guilbaud, M. N. (2017). Paleomagnetically inferred ages of a cluster of Holocene monogenetic eruptions in the tacámbaro-puruarán area (Michoacán, méxico): Implications for volcanic hazards. *J. Volcanol. Geotherm. Res.* 347, 360–370. doi:10.1016/j.jvolgeores.2017.10.004

Mahgoub, A. N., Reyes-Guzmán, N., Bo¨ hnel, H., Siebe, C., Pereira, G., and Dorison, A. (2018). Paleomagnetic constraints on the ages of the Holocene malpaís de Zacapu lava flow eruptions, Michoacán (Mexico): Implications for archeology and volcanic hazards. *Holocene* 28, 229–245. doi:10.1177/0959683617721323

Manea, V. C., Manea, M., and Ferrari, L. (2013). A geodynamical perspective on the subduction of Cocos and Rivera plates beneath Mexico and Central America. Moho: 100 years after andrija mohorovicic. *Tectonophysics* 609, 56–81. doi:10.1016/j.tecto.2012.12.039

Márquez, A., Oyarzun, R., de Ignacio, C., and Doblas, M. (2001). Southward migration of volcanic activity in the central Mexican volcanic belt: Asymmetric extension within a two-layer crustal stretching model. *J. Volcanol. Geotherm. Res.* 112, 175–187. doi:10.1016/s0377-0273(01)00240-2

Márquez, A., Oyarzun, R., Doblas, M., and Verma, S. P. (1999a). Alkalic (ocean-island basalt type) and calc-alkalic volcanism in the Mexican volcanic belt: A case for plume-related magmatism and propagating rifting at an active margin? *Geol.* 27, 51–54. doi:10.1130/0091-7613(1999)027<0051:aoibta>2.3.co;2

Márquez, A., Oyarzun, R., Doblas, M., and Verma, S. P. (1999b). Reply (to comment by L. Ferrari and J. Rosas elguera on "alkalic (ocean-island basalt type) and calc-alkalic volcanism in the Mexican volcanic belt: A case for plume-related magmatism and propagating rifting at an active margin?". *Comment Reply. Geo* 27, 1055–1056. doi:10.1130/0091-7613(1999)027<1055:AOIBTA>2.3.CO;2

Mazzarini, F., Ferrari, L., and Isola, I. (2010). Self-similar clustering of cinder cones and crust thickness in the Michoacan–Guanajuato and Sierra de Chichinautzin volcanic fields, Trans-Mexican Volcanic Belt. *Tectonophysics* 486, 55–64. doi:10.1016/j.tecto.2010.02.009

McBirney, A. R., Taylor, H. P., and Armstrong, R. L. (1987). Paricutin re-examined: A classic example of crustal assimilation in calc-alkaline magma. *Contr. Mineral. Pet.* 95, 4–20. doi:10.1007/bf00518026

McDonough, W. F. (1990). Constraints on the composition of the continental lithospheric mantle. *Earth Planet. Sci. Lett.* 101, 1–18. doi:10.1016/0012-821x(90)90119-i

McDonough, W. F., and Sun, S. S. (1995). The composition of the Earth. *Chem. Geol.* 120, 223–253. doi:10.1016/0009-2541(94)00140-4

McKenzie, D., and O´Nions, R. K. (1991). Partial melt distributions from inversion of rare Earth element concentrations. *J. Petrology* 32, 1021–1091. doi:10.1093/petrology/32.5.1021

Mennella, L., Garduño-Monroy, V. H., Giner Robles, J. L., Liotta, D., and Brogi, A. (2022). Definición del campo de esfuerzos-deformación y sismotectónica del sistema de fallas Morelia-Acambay, México. *revmexcg.* 39, 82–99. doi:10.22201/cgeo.20072902e.2022.1.1688

Middlemost, E. A. K. (1989). Iron oxidation ratios, norms and the classification of volcanic rocks. *Chem. Geol.* 77, 19–26. doi:10.1016/0009-2541(89)90011-9

Molnar, P., and Sykes, L. R. (1969). Tectonics of the caribbean and Middle America regions from focal mechanisms and seismicity. *Geol. Soc. Am. Bull.* 80, 1639–1684. doi:10.1130/0016-7606(1969)80[1639:totcam]2.0.co;2

Moore, G., Marone, C., Carmichael, I. S. E., and Renne, P. (1994). Basaltic volcanism and extension near the intersection of the Sierra Madre volcanic province and the Mexican Volcanic Belt. *Geol. Soc. Am. Bull.* 106, 383–394. doi:10.1130/0016-7606(1994)106<0383:bvaent>2.3.co;2

Mooser, F., and Maldonado-Koerdell, M. (1961). Tectonica penecontemporánea a lo largo de la costa mexicana del Océano Pacífico. *GeofInt.* 1, 1–20. doi:10.22201/igeof.00167169p.1961.1.1.1167

Negendank, J. F., Emmermann, W. R., Krawczyk, R., Mooser, F., Tobschall, H., and Werle, D. (1985). Geological and geochemical investigations on the eastern Trans-Mexican belt. *Geof. Int.* 24, 477–575. doi:10.22201/igeof.00167169p

Ortega-Gutiérrez, F., Gómez-Tuena, A., Elías-Herrera, M., Solari, L. A., Reyes-Salas, M., and Macías-Romo, C. (2014). Petrology and geochemistry of the Valle de Santiago lower- crust xenoliths: Young tectonothermal processes beneath the central Trans-Mexican volcanic belt. *Lithosphere* 6, 335–360. doi:10.1130/l317.1

Osorio-Ocampo, S., Macías, J. L., Pola, A., Cardona-Melchor, S., Sosa-Ceballos, G., Garduño-Monroy, V. H., et al. (2018). The eruptive history of Pátzcuaro Lake area in the Michoacán Guanajuato Volcanic Field, central México: Field mapping, C-14 and $^{40}Ar/^{39}Ar$ geochronology. *J. Volcanol. Geotherm. Res.* 358, 307–328. doi:10.1016/j.jvolgeores.2018.06.003

Ownby, S. E., Delgado-Granados, H., Lange, R. A., and Hall, C. M. (2007). Volcán Tancítaro, Michoacán, México. $^{40}Ar/^{39}Ar$ constraints on its histowy of sector collapse. *J. Volcanol. Geo. Res.* 161, 1–14. doi:10.1016/j.jvolgeores.2006.10.009

Ownby, S. E., Lange, R. A., Hall, C. M., and Delgado-Granados, H. (2011). Origin of andesite in the deep crust and eruption rates in the Tancítaro–Nueva Italia region of the central Mexican arc. *Geol. Soc. Am. Bull.* 123, 274–294. doi:10.1130/b30124.1

Pacheco, J. F., and Singh, S. K. (2010). Seismicity and state of stress in Guerrero segment of the Mexican subduction zone. *J. Geophys. Res.* 155, B01303. doi:10.1029/2009jb006453

Pardo, M., and Suárez, G. (1995). Shape of the subducted Rivera and Cocos plates in southern Mexico: Seismic and tectonic implications. *J. Geophys. Res.* 100, 12357–12373. doi:10.1029/95jb00919

Pasquarè, G., Ferrari, L., Covelli, P., and De Agostini, G. (1991). Geologic map of the central sector of the Mexican volcanic belt, states of guanajuato and michoacan, Mexico. *Geol. Soc. Am. Map Chart Ser.* 72 (1), 20. scale 1:300, 000 (p. text.

Pearce, J. A. (2008). Geochemical fingerprinting of oceanic basalts with applications to ophiolite classification and the search for Archean oceanic crust. *Lithos* 100, 14–48. doi:10.1016/j.lithos.2007.06.016

Pearson, D. G., Brenker, F. E., Nestola, F., McNeill, J., Nasdala, L., Hutchison, M. T., et al. (2014). Hydrous mantle transition zone indicated by ringwoodite included within diamond. *Nature* 507, 221–224. doi:10.1038/nature13080

Peccerillo, A., and Taylor, S. R. (1976). Geochemistry of eocene calc-alkaline volcanic rocks from the kastamonu area, northern Turkey. *Contr. Mineral. Pet.* 58, 63–81. doi:10.1007/bf00384745

Pérez-Orozco, J. D., Sosa-Ceballos, G., Garduño-Monroy, V. H., and Avellán, D. R. (2018). Felsic-intermediate magmatism and brittle deformation in Sierra del Tzirate (Michoacán-Guanajuato Volcanic Field). *J. South Am. Earth Sci.* 85, 81–96. doi:10.1016/j.jsames.2018.04.021

Pola, A., Macías, J. L., Garduño-Monroy, V. H., Osorio-Ocampo, S., and Cardona-Melchor, S. (2014). Succesive collapses of the el estribo volcanic complex in the pátzcualo lake, Michoacán, Mexico. *J. Geo. Res.* 289, 41–50. doi:10.1016/j.jvolgeores.2014.10.011

Pola, A., Macías, J. L., Osorio-Ocampo, S., Sosa-Ceballos, G., Garduño-Monroy, V. H., and Martínez-Martínez, J. (2015). El estribo volcanic complex: Evolution from a shield volcano to a cinder cone, pátzcuaro lake, Michoacán, méxico. *J. Volcanol. Geotherm. Res.* 303, 130–145. doi:10.1016/j.jvolgeores.2015.07.032

Ramírez-Uribe, I., Siebe, C., Chevrel, M. O., and Fisher, C. T. (2021). Rancho Seco monogenetic volcano (Michoacán, Mexico): Petrogenesis and lava flow emplacement base don LiDAR images. *J. Volcanol. Geotherm. Res.* 411, 107169. doi:10.1016/j.jvolgeores.2020.107169

Ramírez-Uribe, I., Siebe, C., Salinas, S., Guilbaud, M. N., Layer, P., and Benowitz, J. (2019). ^{14}C and ^{40}Ar/^{39}Ar radiometric dating and geologic setting of Young lavas of Rancho Seco and Mazcuta volcanoes hosting archaeological sites at the margins of the Pátzcuaro and Zacapu lake basins (central Michoacán, Mexico). *J. Volcanol. Geotherm. Res.* 388, 106674. doi:10.1016/j.jvolgeores.2019.106674

Rasoazanamparany, C., Widom, E., Siebe, C., Guilbaud, M., Spicuzza, M. J., Valley, J. W., et al. (2016). Temporal and compositional evolution of Jorullo volcano, Mexico: Implications for magmatic processes associated with a monogenetic eruption. *Chem. Geol.* 434, 62–80. doi:10.1016/j.chemgeo.2016.04.004

Reubi, O., and Blundy, J. (2009). A dearth of intermediate melts at subduction zone volcanoes and the petrogenesis of arc andesites. *Nature* 461, 1269–1273. doi:10.1038/nature08510

Reyes-Guzmán, N., Siebe, C., Chevrel, O. M., and Pereira, G. (2021). Late Holocene Malpaís de Zacapu (Michoacán, Mexico) andesitic lava flows: Rheology and eruption properties base don LiDAR image. *Bull. Volcanol.* 83, 28. doi:10.1007/s00445-021-01449-0

Robin, C. (1982). "Mexico," in *Andesites*. Editor R. S. Thorpe (Chichester: John Wiley).

Rollinson, H. R. (1993). *Using geochemical data: Evaluation, presentation, interpretation*. Essex, UK: Longmang Scientific Technical.

Rosales-Rivera, M., Díaz-González, L., and Verma, S. P. (2019). Evaluation of nine USGS reference materials for quality control through Univariate Data Analysis System. *UDASys3. Arab. J. Geo.* 12, 40. doi:10.1007/s12517-018-4220-0

Rowe, M. C., Peate, D. W., and Peate, I. U. (2011). An investigation into the Nature of the magmatic plumbing system ar Paricutin Volcano, Mexico. *J. Petro.* 52, 2187–2220. doi:10.1093/petrology/egr044

Rudnick, R., and Fountain, D. M. (1995). Nature and composition of the continental crust: A lower crustal perspective. *Rev. Geophys.* 33, 267–309. doi:10.1029/95rg01302

Rudnick, R. L., and Gao, S. (2003). Compostion of the continental crust. *Treatise Geochem.* 3, 659. doi:10.1016/b0-08-043751-6/03016-4

Schaaf, P., Heirich, W., and Besch, T. (1994). Composition and Sm-Nd isotopic data of the lower crust beneath san Luis Potosí, Central Mexico: Evidence from a granulite-facies xenolith suite. *Chem. Geol.* 118, 63–84. doi:10.1016/0009-2541(94)90170-8

Sheth, H. C., Torres-Alvarado, I. S., and Verma, S. P. (2000). Beyond subduction and plumes: A unified tectonic-petrogenetic model for the Mexican volcanic belt. *Int. Geol. Rev.* 42, 1116–1132. doi:10.1080/00206810009465129

Siebe, C., Guilbaud, M. N., Salinas, S., Kshirsagar, P., Chevrel, M. O., De la Fuente, J. R., et al. (2014). "Monogenetic volcanism of the michoacán-guanajuato volcanic field: Maar craters of the Zacapu Basin and the domes, shields and scoria cones of the tarascan highlands (Paracho-Paricutín region)," in Pre-meeting fieldtrip for the 5th International Maae Conference, Que´retaro, México, November 13-17, 2014 (IAVCEL: Universidad Nacional Autónoma de México).40

Singh, S. K., and Pardo, M. (1993). Geometry of the Benioff zone and state of stress in the overriding plate in central Mexico. *Geophys. Res. Lett.* 20 (14), 1483–1486. doi:10.1029/93gl01310

Sisson, T. W., and Grove, T. L. (1993). Experimental investigations of the role of H2O in calc-alkaline differentiation and subduction zone magmatism. *Contr. Mineral. Pet.* 113, 143–166. doi:10.1007/bf00283225

Sisson, T. W. (2015). "Origins of calc-alkaline (sl) andesitic magmas-where we stand today," in AGU Fall Meeting Abstracts, San Francisco, 14-18 December. V22A-01.2015

Smith, I. E. M. (2013). "High-magnesium andesites: The example of the papuan volcanic arc," in *Orogenic andesites and crustal growth*. Editors A. Gómez-Tuena, S. M. Straub, and G. F. Zellmer (London, United Kingdom: Geological Society, London, Special Publications), 385.

Sosa-Ceballos, G., Boijseauneau-López, M. E., Pérez-Orozco, J. D., Cifuentes-Nava, G., Bólos, X., Peron, M., et al. (2021). Silicic magmas in the Michoacán-Guanajuato volcanic field: An overview of plumbing systems, crystal storage, and genetic processes. *Rev. Mex. Cie. Geo.* 38, 210–225. doi:10.22201/cgeo.20072902e.2021.3.1668

Straub, S. M., Gómez-Tuena, A., Stuart, F. M., Zellmer, G. F., Espinasa-Perena, R., Cai, Y., et al. (2011). Formation of hybrid arc andesites beneath thick continental crust. *Earth Planet. Sci. Lett.* 303, 337–347. doi:10.1016/j.epsl.2011.01.013

Straub, S. M., Zellmer, G., Gómez-Tuena, A., Espinas-Pereña, R., Martín-del Pozzo, A. L., Stuart, F. M., et al. (2014). "A genetic link between silicic slab components and calc-alkaline arc volcanism in central Mexico," in *Orogenic andesites and crustal growth*. Editors A. Gómez-Tuena, S. M. Straub, and G. F. Zellmer (London, United Kingdom: Geological Society London, Special Publications), 385, 31–64.

Suarez, G., and Singh, S. K. (1986). Tectonic interpretation of the Trans-Mexican volcanic belt-discussion. *Tectonophysics* 127, 155–158. doi:10.1016/0040-1951(86)90084-3

Suhardja, S. K., Grand, S. P., Wilson, D., Guzman-Speziale, M., Gomez-Gonzalez, J. M., Dominguez-Reyes, T., et al. (2015). Crust and subduction zone structure of Southwestern Mexico. *J. Geophys. Res. Solid Earth* 120, 1020–1035. doi:10.1002/2014jb011573

Suter, M. (2016). Structure and Holocene rupture of the Morelia fault, Trans-Mexican volcanic belt, and their significance for seismic-hazard assessment. *Bull. Seismol. Soc. Am.* 106, 2376–2388. doi:10.1785/0120160092

Torres-Alvarado, I. S., and Verma, S. P. (2003). Discussion and reply: Neogene volcanism at the front of the central Mexican volcanic belt: Basaltic andesites to dacites, with contemporaneous shoshonites and high-TiO_2, lava. *Geol. Soc. Am. Bull.* 115, 1020–1024. doi:10.1130//B25276D.1

Valentine, G. A., and Connor, C. B. (2015). "Basaltic volcanic fields," in *Encyclopedia of volcanoes*. Editors H. Sigurdsson, B. F. Houghton, S. R. McNutt, H. Rymer, and J. Stix. 2nd edn. (London: Academic), 423–439.

Velasco-Tapia, F., and Verma, S. P. (2013). Magmatic processes at the volcanic front of Central Mexican Volcanic Belt: Sierra de Chichinatuzin volcanic field (Mexico). *Turk. J. Earth Sci.* 22, 32–60. doi:10.3906/yer-1104-9

Verma, S. K., Oliveira, E. P., and Verma, S. P. (2015). Plate tectonic settings for Precambrian basic rocks from Brazil by multidimensional tectonomagmatic discrimination diagrams and their limitations. *Int. Geol. Rev.* 57, 1566–1581. doi:10.1080/00206814.2014.961975

Verma, S. K., Pandarinath, K., and Verma, S. P. (2012). Statistical evaluation of tectonomagmatic discrimination diagrams for granitic rocks and proposal of new discriminant function–based multi–dimensional diagrams for acid rocks. *Int. Geol. Rev.* 54, 325–347. doi:10.1080/00206814.2010.543784

Verma, S. P. (2002). Absence of Cocos plate subduction-related basic volcanism in southern Mexico: A unique case on earth? *Geol.* 30, 1095–1098. doi:10.1130/0091-7613(2002)030<1095:aocpsr>2.0.co;2

Verma, S. P., and Agrawal, S. (2011). New tectonic discrimination diagrams for basic and ultrabasic volcanic rocks through log-transformed ratios of high field strength elements and implications for petrogenetic processes. *Rev. Mex. Cienc. Geol.* 28, 24–44.

Verma, S. P. (2009). continental rift setting for the central part of the Mexican volcanic belt: A statistical approach. *Op. Geol. J.* 3, 8–29. doi:10.2174/1874262900903010008

Verma, S. P. (2006). Extension-related origin of magmas from a garnet-bearing source in the Los Tuxtlas volcanic field, Mexico. *Int. J. Earth Sci.* 95, 871–901. doi:10.1007/s00531-006-0072-z

Verma, S. P. (2000). Gechemistry of the subducting Cocos plate and the origin of subduction-unrelated mafic volcanism at the volcanic fromt of the central Mexican Volcanic Belt. *GSA Sp. Pap.* 334, 195–222. doi:10.1130/0-8137-2334-5.195

Verma, S. P., Guevara, M., and Agrawal, S. (2006). Discriminating four tectonic settings: Five new geochemical diagrams for basic and ultrabasic volcanic rocks based on log — Ratio transformation of major-element data. *J. Earth Syst. Sci.* 115, 485–528. doi:10.1007/bf02702907

Verma, S. P., and Hasenaka, T. (2004). Sr, Nd and Pb isotopic and trace element geochemical constraints for a veined-mantle source of magmas in the Michoacán-Guanajuato Volcanic Field, west-central Mexican Volcanic Belt. *Geochem. J.* 38, 43–65. doi:10.2343/geochemj.38.43

Verma, S. P., Pandarinath, K., Verma, S. K., and Agrawal, S. (2013). Fifteen new discriminant-function-based multi-dimensional robust diagrams for acid rocks and their application to Precambrian rocks. *Lithos* 168-169, 113–123. doi:10.1016/j.lithos.2013.01.014

Verma, S. P. (2015). Present state of knowledge and new geochemical constraints on the central part of the Mexican Volcanic Belt and comparison with the Central American Volcanic Arc in terms of near and far trench magmas. *Turk. J. Earth Sci.* 24, 399–460. doi:10.3906/yer-1504-20

Verma, S. P., and Rivera-Gómez, M. A. (2013). Computer programs for the classification and nomenclature of igneous rocks. *Episodes* 36, 115–124. doi:10.18814/epiiugs/2013/v36i2/005

Verma, S. P. (2020). *Road from geochemistry to geochemometrics*. Singapore: Springer.

Verma, S. P. (2004). Solely extension-related origin of the eastern to west-central Mexican Volcanic Belt (Mexico) from partial melting inversion model. *Curr. Sci.* 86, 713–719.

Verma, S. P. (2010). Statistical evaluation of bivariate, ternary and discriminant function tectnonomagmatic discrimination diagrams. *Turk. J. Earth Sci.* 19, 185–238. doi:10.3906/yer-0901-6

Verma, S. P., and Verma, S. K. (2013). Firsr 15 probability-based multi-dimensional discrimination diagrams for intermediate magmas and their robustness against post-emplacement compositional changes and petrogenetic processes. *Turk. J. Earth. Sci.* 22, 931–995. doi:10.3906/sag-1303-87

Verma, S. P., and Verma, S. K. (2018). Petrogenetic and tectonic implications of major and trace element and radiogenic isotope geochemistry of Pliocene to Holocene rocks from the Tacaná Volcanic Complex and Chiapanecan Volcanic Belt, southern Mexico. *Lithos* 312-313, 274–289. doi:10.1016/j.lithos.2018.05.016

Wanke, M., Clynne, M. A., von Quadt, A., Vennemann, T. W., and Bachmann, O. (2019). Geochemical and petrological diversity of mafic magmas from Mount St. Helens. *Contrib. Mineral. Pet.* 174, 10. doi:10.1007/s00410-018-1544-4

Wanke, M., Karakas, O., and Bachmann, O. (2019b). The genesis of arc dacites: The case of mount st. Helens, WA. *Contrib. Mineral. Pet.* 174, 7. doi:10.1007/s00410-018-1542-6

Wilcox, R. E. (1954). Petrology of paricutín volcano Mexico. *U.S. geo. su. bu.* 965-C, 281–353. doi:10.3133/b965C

Zindler, A., and Hart, S. (1986). Chemical geodynamics. *Annu. Rev. Earth Planet. Sci.* 14, 493–571. doi:10.1146/annurev.ea.14.050186.002425

Zou, H. (2007). *Quantitative geochemistry*. London, England: Imperial College Press.